THIRTEENTH EUROPEAN ROTORCRAFT FORUM

6.14
Paper No. 100

THE PREDICTION OF ROTOR BLADE STRESSES BY THE RAE/WHL COUPLED MODES ANALYSIS

C. YOUNG

MATERIALS AND STRUCTURES DEPARTMENT
ROYAL AIRCRAFT ESTABLISHMENT
FARNBOROUGH, HAMPSHIRE, ENGLAND

September 8-11, 1987
ARLES, FRANCE

ASSOCIATION AERONAUTIQUE ET ASTRONAUTIQUE DE FRANCE

THE PREDICTION OF ROTOR BLADE STRESSES BY THE RAE/WHL COUPLED MODES ANALYSIS

C. Young
Materials and Structures Department
Royal Aircraft Establishment
Farnborough, Hampshire, England

ABSTRACT

The methods developed in the UK for predicting the control system loads, airloads and stresses on a helicopter rotor blade are described. The first generation analysis could treat only simple hub and blade configurations and was superseded in the early 1980s by a comprehensive second generation analysis. The later method is much more versatile than the original and is applied in this paper to the prediction of the blade stresses on five different rotor systems at both model and full scale. The configurations considered are the Puma main rotor fitted with standard and swept tip blades, the SA349/2 research Gazelle main rotor, and a split load path model rotor fitted with rectangular and swept tip blades. The level of correlation between the theory and the test data varies widely and some explanation is offered as to why the analysis performs better on some rotor systems than on others.

1 INTRODUCTION

The flight envelope of a helicopter is limited by many factors which vary with the speed and all up weight of the aircraft. The installed power for example may limit operations at low speed and high gross weight but in high speed flight the most likely limitations are the level of loads in the control system or the stresses in some critical part of the rotor hub or blade. An accurate assessment of the control loads and stresses is therefore essential in the design phase otherwise the aircraft may suffer performance penalties when it enters service.

The prediction of the loads on a helicopter rotor blade is not a simple task. The blades are flexible and so the way they bend, particularly in torsion, affects the loading. The aerodynamic flow field is also complicated because of the wake trailed by the blades and the influence of the fuselage. The aerodynamics are unsteady with Mach number ranging from zero to transonic introducing the problems of drag rise at high speed and dynamic stall on the retreating side of the disc. The rotor dynamics and aerodynamics are also closely coupled, thus predicting the response of the blades is a truely aeroelastic problem.

The first attempt in the UK to produce a method for calculating rotor loads was made by Westland Helicopters Limited (WHL) and is outlined briefly in section 2. The analysis treated only straight blades with either a hinged or built-in root end. The method was extensively modified over the years and thus became somewhat unwieldy towards the end of its life. A new analysis was therefore developed jointly by RAE and WHL which was capable of dealing with the more complicated hub configurations and blade geometries that were envisaged as possible candidates for advanced rotor systems. The features included in the second generation analysis are described in section 3.

The validation of any new analysis is an important stage in the overall development process and must be completed before the method can be used with confidence. The rotor loads calculation is no exception and a great deal of work has already been reported using stresses measured in flight tests with full scale rotors[2] and in wind-tunnel tests of a model rotor[3]. The predicted airloads are also compared with measurements derived from flight test experiments in Ref 4 but this is a more difficult exercise because of the problems associated with integrating a pressure distribution defined by a limited number of sensors.

This paper presents a further series of comparisons between measured and calculated blade stresses, a majority of which have not been published previously. The main rotor of the Puma helicopter fitted with standard blades is considered in section 4 for a range of advance ratios and, five different rotor systems at one advance ratio are used in section 5 to show how varying the hub configuration and blade geometry affects the capability of the analysis. The conclusions drawn from the comparisons are discussed in section 6 with work that is either in hand or planned to improve the method.

2 THE FIRST GENERATION ANALYSIS

The original method for calculating the loads on a rotor blade[1] was limited in the early stages of its development by the speed and storage capacity of available computers. The analysis was extended by WHL however as improved computing facilities became more widespread.

The flexibility of the blades was represented by coupled modes calculated by the method of Isakson and Eisley[5]. The blade was divided into a number of segments with the mass concentrated at the centre. The bending stiffnesses, torsional stiffness and blade pitch were assumed constant between the masses with the twist accounted for by a relative rotation of adjacent segments. The equations were solved by a matrix transfer technique with appropriate boundary conditions imposed for different root configurations. The main limitations of the method were that only straight blades could be treated and there was no provision for a control circuit.

The forced response equation was particularly simple with only aerodynamic and Coriolis forcing terms but a lag damper and a variation of the control system stiffness could be included as options. A cyclic stiffening integral was added at a later date to account for the difference between the azimuthally varying blade pitch angle and the pitch at which the modes were calculated but the inclusion of this term did not always prove beneficial[6]. The forced response equation was solved by a Z-transform forward integration technique with a zero order hold. This was similar to a Laplace transform but used sampled not continuous data and assumed that the forcing did not change between samples.

There was no representation in the analysis of unsteady aerodynamics for either attached or separated flow. The aerofoil lift, drag and pitching moment coefficients were obtained from look up tables which were extremely tedious to prepare. An additional limitation was that only one aerofoil section along the blade was permitted.

The induced velocity over the disc was calculated by one of two options, Glauert or the vortex ring model[7]. The Glauert distribution had a simple triangular shaped variation from the front to the back of the disc but the vortex ring model attempted to represent the wake more realistically. A series of

vortex rings originating from the root and tip, with a half vortex ring at the reference blade, were spaced uniformly vertically and downstream to approximate the spiral vortex pattern. The rings had a prescribed strength which permitted the induced velocity to be evaluated in a closed form expression involving elliptic integrals. The main advantage of this method was its computational efficiency, a major consideration when early mainframe computers were used.

The analysis did not perform any sort of aircraft or rotor trim but simply used the collective and cyclic pitch angles as input data to calculate the rotor thrust and flapping. Convergence to a prescribed set of flight conditions was performed using another computer program in an iterative manner which proved both inconvenient and time consuming.

The first generation analysis was used extensively for more than a decade with many minor improvements incorporated over the years. Much work was done to improve the wake model in particular but the computer program was becoming incomprehensible since it was neither well organised nor in modular form. The decision was therefore taken to replace it with a more comprehensive analysis that was more rigorously derived and which was capable of treating a wider range of rotor systems.

3 THE SECOND GENERATION ANALYSIS

3.1 The blade modes

A modal approach is adopted for the second generation analysis because it facilitates the interpretation of the calculations, especially when a problem is encountered, and is less time consuming compared to other methods such as finite element representations. The new modes calculation, developed by WHL[8], however is very different to that used in the original analysis.

The locus of the blade shear centre is modelled by a series of up to 24 straight line segments which can be orientated in any direction, thus cone and sweep can be introduced at any point along the blade. Secondary load paths are represented by systems of linear and rotational springs. The springs may be attached directly to the blade or may be positioned at the end of a weightless arm. The control circuit of the rotor is usually modelled by a remote spring with the arm having the same geometry as the pitch horn. Point flexibilities can also be included anywhere along the blade to represent pseudo hinges. The root end condition can be built-in for hingeless rotors or have up to three mutually perpendicular hinges, with or without restraint. The modes can also be calculated with steady loads applied as opposed to the more usual method of calculating in vacuo modes. The inclusion of the steady loads means that the displacement of the modes in the forced response solution take the form of small pertubations about the steady state position.

The equations for the blade modes are solved by integrating from the tip to the root, making the appropriate transformations when crossing from one blade segment to another with a different orientation. The trapezium method of integration is used since there is no advantage to be gained from assuming the blade to consist of uniform elements or weightless bays as in the original method. The blade properties such as the mass or stiffness can vary quite generally and change rapidly over short distances without loss of accuracy.

3.2 The forced response equation

The forced response equation is fully compatible with the blade modes and is derived to a consistent order of accuracy throughout. There are five main forcing terms in the equation arising from the Coriolis force, the cyclic inertia force, the cyclic stiffening, the non-linear terms and the aerodynamics. A lag damper and a variation of the control system stiffness can also be included.

The forcing due to the blade dynamics is fairly easy to evaluate as it is composed of functions of modal displacements, slopes and curvatures. The difficulty lies with the aerodynamic forcing since it must take into account unsteady aerodynamic effects, the rotor wake and the fuselage flow field. The design of modern blades is also complicated aerodynamically and the method allows for a spanwise variation of aerofoil section with a maximum of eight sections varying linearly or discontinuously over the blade.

The unsteady aerodynamic effects are modelled by Wagner functions for attached flow and there are two possible representations of dynamic stall. One method uses a time delay model[9] which assumes that there are two distinct time constants which determine when the lift and pitching moment coefficients diverge once the aerofoil exceeds the static angle for maximum lift. The other dynamic stall model uses a leading-edge velocity criterion[10] but is applicable only at low Mach number.

The rotor induced velocity distribution can be calculated by one of four methods; Glauert, vortex ring, vortex ring with an interactive near wake, and a spiral vortex model. The Glauert method is unchanged from that used in the original analysis but the vortex ring model has undergone extensive modification particularly in the positioning of the rings both horizontally and vertically. The wake can also be contracted in which case the model assumes that the complete vortex rings have a prescribed radius less than the blade radius. The interactive near wake, which is used in conjunction with the vortex ring model, replaces the two half rings originating from the reference blade with a series of half rings whose strength is related to the load on the blade. This overcomes the problem of excessive amounts of negative loading near the tip on the advancing side of the disc in high speed flight which occurs when the vortex ring model is used alone. The development of the vortex ring model and the interactive near wake is described in Ref 11. The spiral vortex wake model is not used very frequently because it is too time-consuming for use on a regular basis. The method models the undistorted spiral path of the wake using curved vortex elements in a similar manner to that developed for the wake in hover[12].

The fuselage flow field can be calculated internally in the analysis using a single source or externally using a panel method. The panel method is preferred because it allows a better representation of the fuselage shape. The inclusion of the fuselage has a considerable effect on the predicted loads and vibrational characteristics of a rotor[13] and is represented whenever possible.

The forced response equation is solved by the Z-transform technique as in the original analysis but a first order hold is included as an option. This hold circuit assumes that the forcing changes linearly between samples and reduces the azimuth error associated with the zero order hold.

The blade loads are currently calculated by modal summation but the unified formulation[14] is to be included in the near future to improve the prediction of the localised loading effect of lag dampers.

3.3 Trimming the rotor

There are two versions of the new analysis, one considering an isolated rotor and the other the complete aircraft. The isolated rotor computer program has four trim options:

(i) collective and cyclic pitch angle specified;

(ii) rotor thrust and first harmonic flapping angles specified;

(iii) rotor thrust and first harmonic flapwise or flatwise bending moment specified;

(iv) rotor thrust and first harmonic secondary load path force specified.

The second option is normally used for articulated rotors when making comparisons with measured data and the bending moment trim option for hingeless rotors.

The computer program for the complete aircraft uses the analysis described above for both the main and tail rotor, although a simpler treatment for the tail rotor is also included as an option. The calculation provides a force and moment balance for the helicopter in steady rectilinear flight but the modelling of some of the interactions, *eg* the main rotor wake on the tail rotor, has yet to be completed.

4 THE STRESSES ON THE PUMA MAIN ROTOR BLADE

The analysis is applied first to the main rotor of the Aerospatiale Puma helicopter which is the research aircraft of Flight Systems Department, RAE Bedford.

The Puma main rotor has articulated blades with a hinge offset of 3.7% radius. The rotor radius is 7.5 m and the blades have an 8° linear twist. The aerofoil section is formed by a NACA 0011.8 profile to 30% chord based on a chord length of 0.5 m with a lengthened aft portion to give a total blade chord of 0.54 m and thus a reduced thickness/chord ratio of 10.93%.

The experimental data presented in this section were obtained at RAE Bedford using an aircraft fitted with standard metal blades. The flatwise bending moment was measured at 35%, 45%, 55%, 65%, 75%, 83%, 90% and 95% radius but only the data at 65% radius, where the maximum stresses were recorded, are considered. The edgewise bending moment was measured at only 73% radius and the torsional moment at 33% and 73% radius, but only the inboard position is used for comparison with the analysis. All the test data are filtered using a cut off frequency of 100 Hz as some of the measurements are very noisy and the mean level has been removed as the datum for the test data differs from the analysis.

Six flight test cases are analysed with the advance ratio increasing from less than 0.1 to more than 0.4. The flight conditions are shown in the following table and each is identified by a run number. All examples are in level flight except for run 8 where the rate of descent is 2.4 m/s.

Run number	4	5	6	7	8	9
Indicated airspeed (knots)	32	62	90	140	160	120
Aircraft mass (kg)	5100	5100	5080	5060	5030	5000
Altitude (metres)	1823	1829	1826	1820	1768	1821
Temperature (degrees C)	0	0	0	0	0	0
Rotor speed (rev/min)	270.27	270.84	270.07	264.58	261.62	267.39
Advance ratio	0.0972	0.1707	0.2414	0.3771	0.4340	0.3210
C_t/solidity	0.0666	0.0663	0.0664	0.0689	0.0696	0.0667

The measured rotor speed, atmospheric conditions, shaft angle, advance ratio and the first harmonic components of the blade flapping are used to define the input to the analysis. The rotor thrust is taken to be the aircraft weight with no correction for the download on the airframe but the fuselage flow field is represented. All the calculations use the vortex ring downwash model with the interactive near wake.

The flatwise bending moments for each case are considered first and Fig 1 compares the measured and predicted moment for run 4 at an advance ratio of 0.0972. The calculation is made with an uncontracted wake and the level of correlation is poor, but contracting the wake to 92% radius, Fig 2, yields some improvement particularly on the retreating side of the disc. A series of calculations made with different contraction ratios for the wake shows that local improvements are possible in other areas of the disc suggesting that the wake is distorting and cannot be represented easily by a fixed contraction.

The correlation between the test data and the analysis for the flatwise bending moment at 65% radius improves when the advance ratio is increased to 0.1707 for run 5, Fig 3. The calculations are made with a wake contraction ratio of 95% for this example but there is still evidence that the wake is distorting.

An uncontracted wake is used in the calculations for the remainder of the flight test cases thus giving a progression from a typical hover wake contraction factor at low advance ratio to an undistorted wake at high forward speed. The analysis agrees well with the test data for run 6, advance ratio 0.2414, Fig 4, except perhaps around the front of the disc where the theory predicts a more pronounced oscillation.

The next test case in the sequence of increasing forward speed is run 9 at an advance ratio of 0.3210. The analysis again correlates well with the measurements, Fig 5. There is a general improvement around the front of the disc compared to the previous example but the peak in the first quadrant is now underestimated.

Increasing the advance ratio to 0.3771 for run 7 produces the comparison between the theory and the test data shown in Fig 6 but note that the scale of the ordinate is changed from the previous illustrations. The analysis does not predict the oscillation around the front of the disc particularly well in this case but elsewhere the level of correlation is satisfactory.

The last flight case considered is run 8 at an advance ratio of 0.4340 which corresponds to an advancing blade tip Mach number of 0.884. The measured and predicted flatwise bending moments at 65% radius, Fig 7, show good correlation. There is some disagreement around the front of the disc as in the previous example but the peak in the first quadrant and on the retreating side of the disc are predicted well.

The flatwise bending moments for the Puma main rotor blade calculated by the RAE/WHL analysis compare well with the test data except at low advance ratio where the fixed contraction ratio of the wake does not model the distortion correctly. The magnitude of the oscillation is predicted accurately at higher speeds even though some of the finer details of the waveform are in error. The examples presented have shown comparisons at only one radial station but a comparable level of correlation is obtained over the complete span of the blade.

The Puma main rotor is fitted with hydraulic lag dampers but these are not represented in the calculations because their characteristics are not known to RAE. This is not too important for the comparisons with the test data as the measurements are made at 73% radius, far removed from the damper attachment point.

The measured and calculated edgewise bending moments for run 4, the lowest advance ratio case, are shown in Fig 8. The calculations display a pronounced 5R oscillation, which is consistent with the calculated second lag mode frequency of 4.74R, whereas the test data has a predominant 4R component. This trend is apparent in all the flight cases considered and suggests that the lag mode frequency may be reduced, possibly by flexibilities in the gearbox. The neglect of the inertia of the transmission in the calculations however, may also be responsible.

An increase in the high frequency content of both the calculated and measured edgewise bending moments, Fig 9, is apparent for run 5. A harmonic analysis of the waveforms shows that the test data has large components at 4R and 13R but the calculations are dominated by oscillations at 5R and 14R. The predicted frequency of the third lag mode is 13.75R which again implies that this mode is detuned in addition to the second lag mode.

The comparison between measurement and calculation for both runs 6 and 9 is very similar to that for run 5 but for run 7 the high frequency content in the test data and the predictions is diminished to a large extent. The high order harmonics remain absent for run 8 at the highest advance ratio, Fig 10, but the difference in the dominant frequency of the measured and calculated waveform is still present.

The comparisons of the edgewise bending moments show that there is some deficiency in the modelling of the behaviour of the rotor in the lagwise sense. This is almost certainly due to the lack of transmission modes in the analysis but it is difficult to draw any firm conclusions with measurements available at only one radial station.

The torsional moments on the blade of a rotor can be difficult to predict and the main factor seems to be the stiffness of the control system relative to the torsional stiffness of the blade, in general the softer the control system the more likely the problems. The control system stiffness of the Puma is relatively low and about 40% of the tip deflection in the first torsional mode occurs at the feathering bearing. The stiffness probably also varies with azimuth thus the correlation between the calculated and measured torsion moment at 33% radius is not very good.

The aerodynamic forcing of the torsion modes dominates at low advance ratio and is due to the change in the pitching moment coefficient whenever there is a vortex interaction. This feature is not modelled particularly well in the current representation of the unsteady aerodynamics with the result that the calculation is in rather poor agreement with the test data, Fig 11, for run 4.

There are fewer vortex interactions when the advance ratio is increased for run 5 and the analysis correlates somewhat better with the test data, Fig 12. The main discrepancy is an underprediction of the 1R component and an overestimation of the fourth harmonic, the latter accounting for the peak around 260° azimuth.

The error in the predicted first harmonic component increases with increasing advance ratio and is more pronounced for run 6, Fig 13. The calculated 4R and 5R harmonics are also too great so that the analysis, while following the trend of the test data, shows a poorer level of correlation than at the lower advance ratio.

The trend in the measurements is not even approximately correct when the advance ratio is increased further, Fig 14 for run 9. The magnitude of all the low order harmonics, first, second and third, is underpredicted and the test data shows a more pronounced 5R component which is absent in the calculation.

The level of correlation becomes progressively worse at the two highest advance ratios as the retreating blade approaches stall, Figs 15 and 16 for runs 7 and 8 respectively. The calculated torsional frequency of the blade is 5.63R and the measurements show increasing amounts of the fifth and sixth harmonic components which have a magnitude more than twice that of the calculations. The predicted lower order harmonics also remain in error and the overall level of agreement with the test data is poor.

The representation of unsteady aerodynamic effects at low advance ratio and the modelling of the control system are the two main reasons why the analysis fails to predict accurately the torsional behaviour of the blade. The theory uses only one torsion mode, a collective mode, but there are likely to be other types of modes, *eg* cyclic and reactionless, that respond in practice. Work is in hand to remedy this deficiency, as described in section 6, but it must be admitted that the calculation of the elastic twisting of the blade for some rotor systems is one of the main limitations of the current analysis.

The results presented in this section have explored the capability of the second generation analysis to predict the blade stresses for one type of rotor system over a range of advance ratio. The flatwise bending moments generally correlate well with the test data except at low advance ratio, where deficiencies in the wake model are apparent, but the representation of the trans-

mission and control system need improvement before good correlation with experiment is obtained for the edgewise bending and torsional moments. These conclusions however, do not necessarily carry over to other rotor systems.

5 THE STRESSES ON FIVE ROTOR SYSTEMS

The measurements made on a conventional articulated rotor system are compared with the predictions over a range of advance ratios in the previous section. Five different rotor and hub configurations are considered in this section at a typical cruise advance ratio to demonstrate how the analysis can cope with more sophisticated geometries.

5.1 The Puma swept tip blade

The Puma results for run 9 discussed previously are used as a baseline for consideration of the comparisons between theory and experiment with the swept tip blades. The initial flight tests[15] compared the measurements made on the advanced geometry tip with those obtained on a rectangular tipped blade but the test data presented in this section are from later flights with the rotor having four identical swept tipped blades.

The swept tip, whose geometry is given in Ref 15, is manufactured by fitting a fairing over the standard blade except that the spar near the tip is cut away to accommodate the sweep. The fairing however, increases the polar moment of inertia of the blade with the result that the fundamental torsional frequency of the blade decreases from about 5.6R to 5.01R. Some other modal frequencies also change but not significantly.

The flight test chosen is made at an advance ratio of 0.326, close to that for the baseline rotor at 0.321, but the thrust coefficient/solidity is 0.0798, somewhat higher than that for run 9. This is the closest comparison that can be achieved as the stress data for the swept tip blade at a similar thrust level to the baseline rotor are unusable.

The comparison between the measured and predicted flatwise bending moment at 65% radius for the baseline rotor is shown in Fig 5 and for the swept tip blade at 62% radius, the nearest comparable measuring station, in Fig 17. The effect of the change in tip geometry, and to a lesser extent the difference in thrust coefficient, is quite evident in the test data. The waveforms have the same basic shape but the magnitude of the oscillation around the front of the disc is larger for the swept tip blade and this is reflected in the predictions to a certain extent. The analysis also predicts the peak in the first quadrant better for the swept tip than for the standard blade but the position is reversed on the retreating side of the disc. The third peak occurs earlier in azimuth for the swept tip blade and this is due to the different aerodynamic loading experienced on the tip compared to the straight blade. This feature is not accounted for fully in the analysis as yet. Generally the level of correlation between the analysis and the test data is fairly good for the swept tip blade but is somewhat degraded relative to the standard blade.

The edgewise bending moment for run 9 with the rectangular tip blade is not included in the illustrations for section 4 and is shown in Fig 18. The test data, at 73% radius, has a strong 4R component whilst theory is dominated by 5R and 14R harmonic components so the correlation is poor. The measurements

with the swept tip are made at 12.2%, 33%, 55%, and 83% radius but the outermost gauge failed so no direct comparison at a similar radial station to the standard blade data can be made. The comparison between theory and experiment at 55% radius, Fig 19, is therefore the closest match. The predictions are primarily a 5R oscillation but its magnitude is very much smaller than the 4R variation in the test data. However, reducing the frequency of the second lag mode close to 4R, to represent the detuning due to the transmission, produces the comparison with the test data shown in Fig 20. The level of correlation is improved significantly with a much larger peak-to-peak moment. The phasing however, is not correct and theory does not show the reduction in the amplitude of the bending moment around the retreating side of the disc.

The measured torsional moment at 33% radius for the swept tip blade, Fig 21, has an amplitude some 60% greater than the standard blade, Fig 14. The characteristic shape of the oscillations are similar however, although the peak around the front of the disc occurs earlier in the cycle for the swept tip blade. The calculations also show an increase in the magnitude of the oscillatory moment for the swept tip blade compared to the standard blade but the increase is insufficient to match the test data. The details of the waveform also compare badly with the measurements for both blades and the correlation is poor.

The swept tip produces some changes in the stresses on the blade compared to the standard rectangular planform. The flatwise bending moments change by the smallest amount and the correlation with the analysis remains fair although not as good as with the standard blade. The edgewise bending moments are predicted poorly unless the frequency of the second lag mode is reduced but the torsional moments are not predicted accurately for either blade.

5.2 The SA349/2 Gazelle helicopter

The SA349/2 Gazelle helicopter is used as a research vehicle by Aerospatiale and has been used to measure performance, blade pressure distributions and blade stresses[16]. The aircraft has an advanced, fully articulated rotor with the 'Non Articule en Trainée' hub and the 'Grande Vitesse' blades. The rotor, though articulated, makes an interesting comparison with the Puma because the arrangement of the hinges is rather unusual. The flap hinge is located at 2.1% radius with the feathering bearing immediately outboard at 4.76% radius. The lag hinge is the most outboard articulation at 9.05% radius but is constrained by a stiff elastomeric damper with a complicated geometry to provide damping for both positive and negative lag angles. The presence of the damper increases the fundamental lag mode frequency to 0.54R, more akin to a soft inplane hingeless rotor than an articulated system. The rigid blade flapping frequency, at 1.02R, however, is typical of a low hinge offset configuration. Another important distinction between the Gazelle and Puma rotor systems lies in the torsional characteristics. The SA349 blades are torsionally soft and the control system stiffness relatively high thus virtually all the twisting occurs in the blade. This is different to the Puma where only 60% of the torsional deflection at the tip occurs in the blade with the remaining 40% arising at the feathering bearing. The Gazelle rotor system is therefore so very different from the conventional articulated rotor as to make it worthy of study.

The flight test case chosen for investigation has an advance ratio of 0.344 and a rotor thrust coefficient/solidity of 0.065. These values are close to run 9 for the Puma fitted with standard blades so that this case can be used again as a baseline.

The measured and calculated flatwise bending moment at 54% radius for the SA349 rotor, the nearest measuring station to the position used for the baseline Puma data, is shown in Fig 22. The correlation between theory and experiment is generally poor, certainly worse than that shown in Fig 5 for the Puma at similar flight conditions. The error in the calculation is due to an underprediction of the amplitude of the second and third harmonic components and an overestimation of the fifth harmonic. Fig 22 is typical of the level of correlation obtained over most of the blade span except that further outboard, typically 80% radius, the position is even worse. This is in marked contrast to the results for the Puma where good agreement with the test data is maintained along the complete span. The reason for the poor performance of the analysis is not clear at present. The blade properties are defined in great detail and the calculated modal frequencies agree with those predicted by other methods. More flight cases therefore need examination to uncover the source of the error.

The edgewise bending moment is measured at 12%, 20%, 46%, 54%, 63%, 80% and 85% radius in the flight tests. The correlations with the calculation are made at 20% radius, near the damper attachment point, and at 54% radius for comparison with the Puma data.

The analysis predicts the bending moment at 20% radius reasonably well with the main error being an underestimate of the amplitude of the second harmonic component, Fig 23. The level of correlation is similar to that obtained for the Lynx[2] rotor, a true soft inplane hingeless rotor, and is better than that observed for articulated rotors near the damper attachment point. This shows that the evaluation of blade loads by modal summation is effective for elastomeric dampers, where the primary damping moment arises from a displacement, whereas the unified formulation[14] or force integration is necessary for viscous dampers where the lagging velocity is the principal source of damping. The situation further outboard is not so clear cut and the comparison between the predicted and measured edgewise bending moment at 54% radius, Fig 24, has some of the characteristics noted in the comparisons with the Puma data, Figs 19 and 20. The predicted second lag mode frequency is 5.15R and the calculated bending moment shows a large 5R oscillation. The test data however, has a relatively small 5R component and the third and fourth harmonics have a greater amplitude. This again suggests a detuning of the second lag mode frequency as with the Puma. Overall however, the level of correlation between theory, with the calculated modal frequencies, and the test data for the edgewise bending moment is much better for the Gazelle than for the Puma, and in particular, the peak-to-peak moments are estimated more accurately.

The torsional moment is predicted badly for the Puma blade, Fig 14, but a much better correlation with the test data is obtained for the SA349 rotor, Fig 25 at 20% radius. The main deficiency is an underestimation of the second harmonic component but both the magnitude and phase of the first harmonic variation is predicted correctly, something rarely obtained on the Puma. The improvement in the correlation is probably due to the reduced influence of the control system for the Gazelle compared to the Puma since even large variations in the control system stiffness have a small effect on the blade torsional frequency.

The results presented in this section show that the type of rotor system has a considerable influence on the performance of the analysis. The flatwise bending moments for the Puma are predicted accurately but the edgewise bending and torsional moments are considerably in error. The position is completely

reversed for the Gazelle rotor system where the correlation between the theory and the test data is poor for the flatwise moments but acceptable for both the edgewise and torsional stresses. A comparison of the two sets of data show that studying rotor systems with different characteristics is invaluable in understanding where the analysis is weak.

5.3 The model rotor

The split load path model rotor for the RAE 24ft Wind Tunnel has the most complicated hub configuration of all the rotor systems analysed to date. The rig is described fully in Ref 17 but basically the aim of a split load path rotor is to separate the structural elements of the rotor that carry the centrifugal force from those that control the fundamental flap and lag frequencies. Such a hub allows the designer more freedom to select the characteristics of the system to provide the qualities required.

A sketch of the hub assembly is shown in Fig 26. The primary load path, which carries the centrifugal load, has a spherical elastomeric bearing at the root allowing flap, lag and pitch motion. The control circuit is attached to the bearing so that the complete primary load path varies in pitch. The load path passes through a coupling bearing and is joined to the blade spar via the swept link. A cage surrounds the coupling bearing and is attached to it by elastomers which provide restraint and damping in lag. Spring like flap flexures are attached to the cage to provide the flapping restraint. The primary load path is modelled in the analysis in the same way as any conventional rotor and the secondary load paths, *ie* the lag elastomers and the flap flexures, by point springs to earth. The calculated first lag and flap frequencies of the rotor are 0.61R and 1.1R respectively which gives the system the characteristics of a soft inplane hingeless rotor.

The blades described in Ref 17 are dynamically scaled but have a relatively high torsional frequency. A different method of blade construction is employed now and the torsional frequency is more representative of full scale rotors. Two blades of the new type are considered, one straight and the other having a simple swept tip. The tip is swept at 20° over the outboard 12% radius, such an exaggerated planform being necessary because the blades are not Mach scaled. The aim of testing the blades is to make a direct comparison between the two planforms but a flutter problem encountered on the swept tip blade[21] could only be cured by adding mass and increasing the torsional stiffness. However, the blades are still sufficiently similar to provide a worthwhile comparison. The main difference between the dynamics of the two blades is the torsional frequency which is 4.96R for the straight and 6.41R for the swept tip blade. The results presented are for an advance ratio of 0.34 at a rotor thrust of 750 N equivalent to a thrust coefficient/solidity of 0.0638. The flight parameters are similar therefore to those for the Puma and SA349 rotors allowing a comparison not only between the blades but also with the full scale rotors.

The measured and calculated flatwise bending moments at 60% radius are shown in Fig 27 for the straight blade and in Fig 28 for the swept tip blade. The correlation between the analysis and the test data for the straight blade is fair but below the level achieved for the Puma rotor. Some of the discrepancy however, may be due to the way in which the rotor is trimmed. The model is controlled by cyclic pitch in the wind tunnel to eliminate the first harmonic component of a force measured about half-way along the flap flexure. This force however, is the difference between the aerodynamic load transmitted by the blade to the end of the flexure and the component of the centrifugal force acting on the heavy cage and coupling bearing. The centrifugal component varies with the

blade flapping thus to match theory to experiment requires accurate prediction of both the aerodynamic loading and the blade flapping response and this is not easy to achieve. The oscillatory blade stress is reduced by the swept tip, Fig 28, and this is reflected in the calculations. The correlation with the test data is also better than for the straight blade especially in the second quadrant.

The calculated and measured edgewise bending moment at 45% radius is shown in Fig 29 for the straight blade. The test data has a more pronounced oscillation coming from the second lag mode compared with the calculations but the amplitude of the low order harmonics is predicted well. The level of blade stress is reduced again by the swept tip, Fig 30, and theory shows a greater excitation of the second lag mode although the phasing is incorrect.

The swept tip has a considerable influence on the torsional motion of the blade and this can be seen by comparing the measured torsion moment at 30.75% radius, Fig 32, with that for the straight blade, Fig 31. The effect of the sweep is to introduce a double peak on the retreating side of the disc and to reduce the nose-down twist in the second quadrant. The analysis underestimates the amplitude of the first harmonic component of the torsion moment for the straight blade and the presence of the second torsion mode at 14.9R confuses the comparison with the test data for the swept tip blade. The calculation shown in Fig 32 does show evidence of a double peak, although the phasing is wrong, and the nose-down moment is reduced on the advancing side of the disc. The trends arising from the change in planform are evident therefore but the overall level of correlation with the measurements is poor for both blades.

The model rotor with its split load path hub is a difficult system to analyse and this is reflected in the reduced level of correlation with the test data compared to rotors with simpler hub configurations. The representation of the secondary load paths by linear springs is probably too simplistic and the analysis may need to include the effects of the inertia of the secondary load path structural elements. Continued testing of the model however, will yield useful information about the dynamics of rotors to aid development of the theoretical methods.

6 DISCUSSION AND FUTURE WORK

The comparisons between the analysis and the test data presented in sections 4 and 5 show that the level of correlation varies considerably from extremely good to very bad. The reason for the variability is discussed in this section with a description of the work that is in hand to remedy the deficiencies.

The predicted blade flatwise stresses for the Puma main rotor at low advance ratio are not very accurate and the airloads are also estimated badly[4]. Improvements are necessary therefore to the modelling of the rotor wake and the unsteady aerodynamics. The strength of the complete vortex rings representing the trailing vorticity from the blades takes a prescribed value. This does not reflect the variation of the blade load particularly well at low speed since the strength does not show the rapid changes associated with vortex interactions. A modification to the existing wake model is possible but a new method is under development which shows more promise. The new model has arisen from investigations into the acoustics of blade slap and consists of a near wake representation[18], a model for blade/vortex interactions[19], and a yet to be developed far wake model.

The reason for considering a new model is the requirement to extend the rotor loads analysis to manoeuvring flight and this may not be possible by modifications to the vortex ring wake model.

The representation of unsteady aerodynamics in the analysis does not model some features of the flow that are important at low advance ratio. In particular the impulsive change in the lift and pitching moment coefficients when a vortex interaction occurs are not included at present. A second generation model[20] is available which includes these and other features but is not yet incorporated into the analysis as further validation against two-dimensional aerofoil data is required. The improved unsteady aerodynamic procedure coupled with the new wake model should improve by a marked degree the calculation of the blade stresses at low speed.

The accuracy of the predicted torsional stresses on the blade varies widely, being poor on the Puma and model rotors but fair for the SA349 blade. The influence of the control system, especially its stiffness relative to the blade torsional rigidity, appears to be important but in reality the situation is far more complicated. A complete rotor system has more types of vibrational modes than the blade collective mode and all the modes have a different path to earth each with an associated stiffness and inertia. The oversimplification of the rotor dynamics is recognised and work is now in progress to develop a coupled rotor/fuselage analysis. The fixed shaft blade analysis will then be replaced by a rotor analysis with hub motion included, such a method being essential for simulating manouevring flight. The new analysis will include the transmission system and, as the initial work points to the need for complex modes, the inclusion of a viscous lag damper will be possible. This should lead to improvements in predicting the edgewise bending moments especially near the blade root for conventional articulated rotor systems.

The development of methods to calculate rotor blade stresses is an evolutionary process and the work outlined above should lead to improvements in areas where the present analysis is known to be weak. Further validation at this stage is then necessary to guide the way ahead.

7 CONCLUSIONS

The second generation RAE/WHL rotor loads analysis has undergone extensive validation and the examples presented in this paper were only a sample. The predictions of the analysis have been compared with measurements from flight tests over a range of advance ratios and for different rotor systems, at both model and full scale, at a typical forward speed for cruise. The level of correlation was variable but some explanation as to why the analysis proved incapable of more accurate prediction was offered in most cases. Improvements to the method were described which will lead to a third generation analysis of even greater capability and applicability.

REFERENCES

1 R. Wilkinson, A description of a computer program to predict the performance of a helicopter rotor in steady forward flight, WHL Research Paper 397 (1971).

2 C. Young, A comparison of the measured and predicted stresses on the rotor blades of three helicopters, RAE Technical Report 85027 (1985).

3 C. Young and P.A. Thompson, A further comparison of the measured and predicted loads on a split load path model helicopter rotor, RAE Technical Report 85095 (1985).

4 C. Young, A comparison of the measured and predicted airloads on the rotor blades of three helicopters, RAE Technical Report to be published.

5 G. Isakson and J.G. Eisley, Natural frequencies in coupled bending and torsion of twisted rotating and nonrotating blades, NASA CR-65 (1964).

6 R.E. Hansford, A comparison of predicted and experimental rotor loads to evaluate cyclic flap-lag coupling, WHL Research Paper 551 (1977).

7 C.V. Cook, Induced flow through a helicopter rotor in forward flight, WHL Research Paper 374 (1970).

8 S.P. King, Blade equations by Hamilton's method using an ordering scheme, Unpublished WHL Report.

9 T.S. Beddoes, A synthesis of unsteady aerodynamic effects including stall hysteresis, Forum Proceedings of the 1st European Rotorcraft and Powered Lift Aircraft Forum, Paper 17, September 1975.

10 T.S. Beddoes, Onset of leading edge separation effects under dynamic conditions and low Mach number, WHL Research Paper 562 (1977).

11 C. Young, Development of the vortex ring wake model and its influence on the prediction of rotor loads, AGARD CP-334 (1982).

12 C. Young, The representation of the helicopter rotor wake in hover, RAE Technical Report 82121 (1982).

13 P.G. Wilby, C. Young and J. Grant, An investigation of the influence of fuselage flow field on rotor loads, and the effects of vehicle configuration, Forum Proceedings of the 4th European Rotorcraft and Powered Lift Aircraft Forum, Paper 8, September 1978.

14 R.E. Hansford, A unified formulation of rotor load prediction methods, Paper presented at the 41st Annual Forum of the American Helicopter Society, Fort Worth, Texas, USA, May 1985.

15 M.J. Riley and Judith V. Miller, Pressure distributions on a helicopter swept tip from flight tests and calculations, Forum Proceedings of the 9th European Rotorcraft Forum, Paper 9, September 1983.

16 Ruth M. Heffernan and M. Gaubert, Structural and aerodynamic loads and performance measurements of an SA349/2 helicopter with an advanced geometry rotor, NASA Technical Memorandum 88370 (1986).

17 J.T. Cansdale, R.J. Marshall and P.A. Thompson, Tests on a new dynamically scaled model rotor in the RAE 24ft Wind Tunnel, Forum Proceedings of the 10th European Rotorcraft Forum, Paper 98, August 1984.

18 T.S. Beddoes, A near wake dynamic model, Paper presented at the National Specialists' Meeting on Aerodynamics and Aeroacoustics, Arlington, Texas, USA, February 1987.

19 T.S. Beddoes, A wake model for high resolution airloads, Paper presented at the International Conference on Rotorcraft Basic Research, Research Triangle Park, North Carolina, USA, February 1985.

20 J.G. Leishman and T.S. Beddoes, A second generation model for aerofoil unsteady aerodynamic behaviour and dynamic stall, WHL Research Paper 704, (1986).

21 W.R. Walker and C. Hatch, Pitch-flap flutter instability of a swept tip model rotor blade, Forum proceedings of the 13th European Rotorcraft Forum, September 1987.

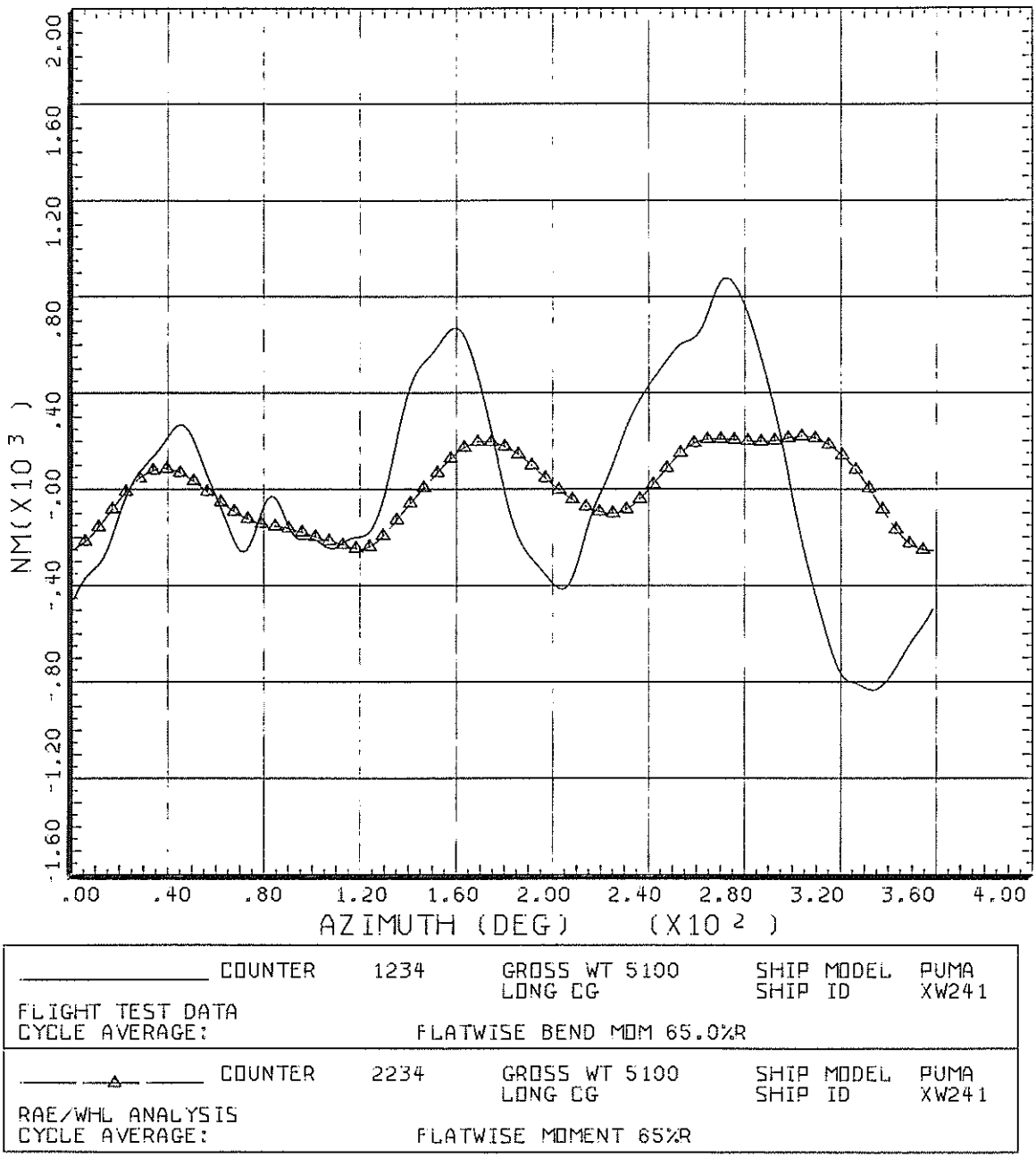

Fig 1 Measured and predicted flatwise bending moment for the Puma main rotor blade, $\mu = 0.0972$

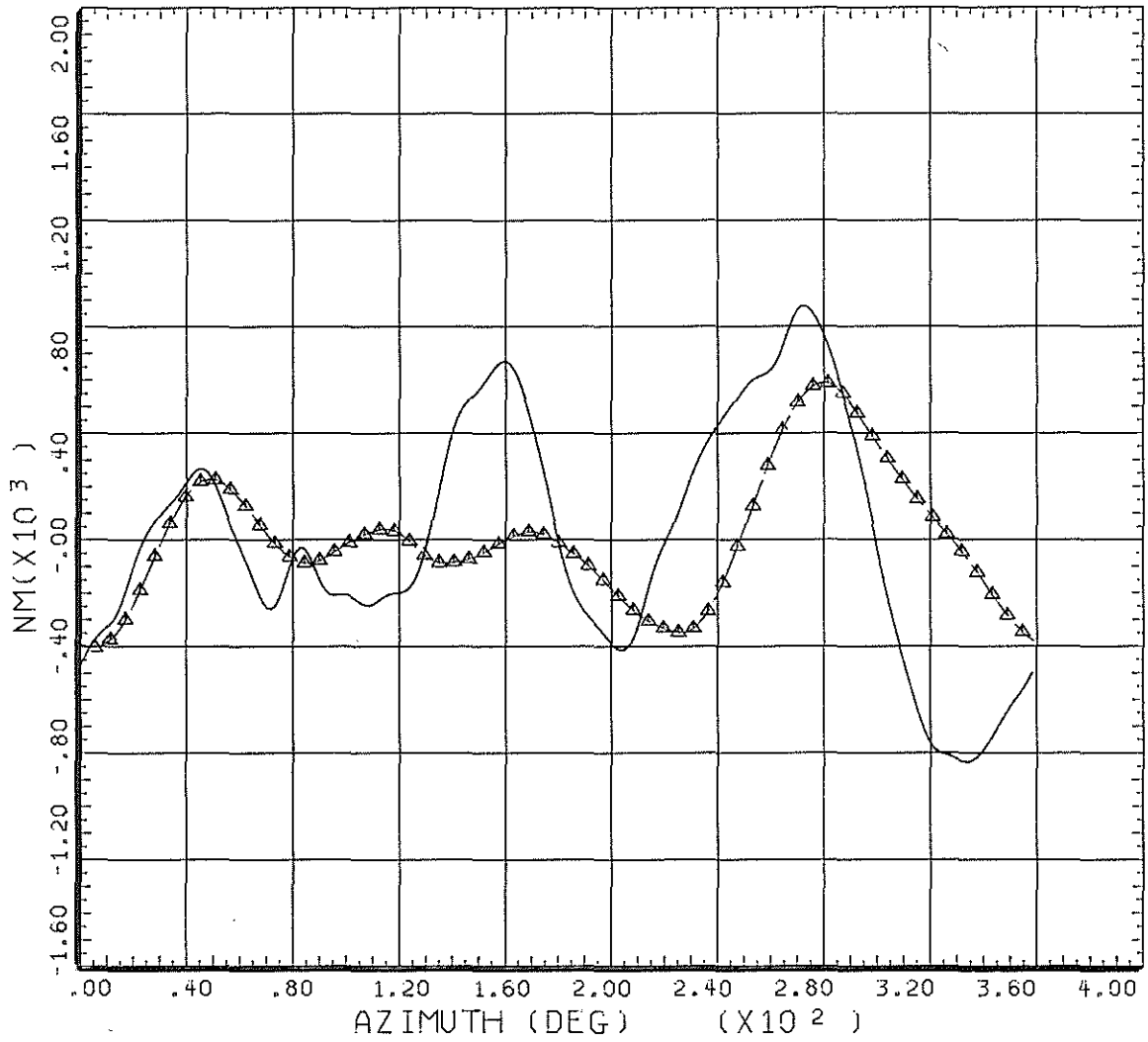

Fig 2 The effect of contracting the wake on the flatwise bending moment, $\mu = 0.0972$

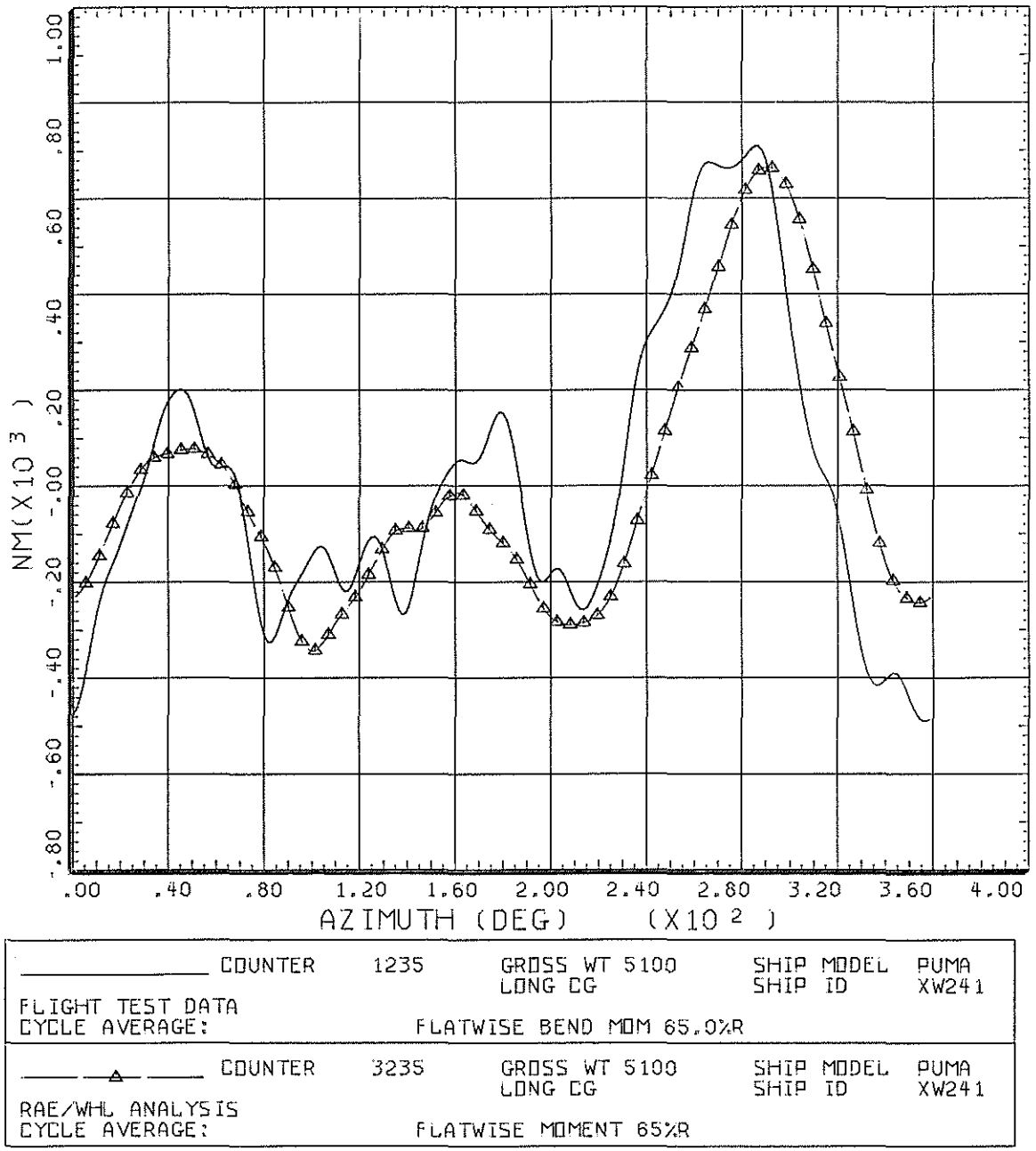

Fig 3 Measured and predicted flatwise bending moment for the Puma main rotor blade, $\mu = 0.1707$

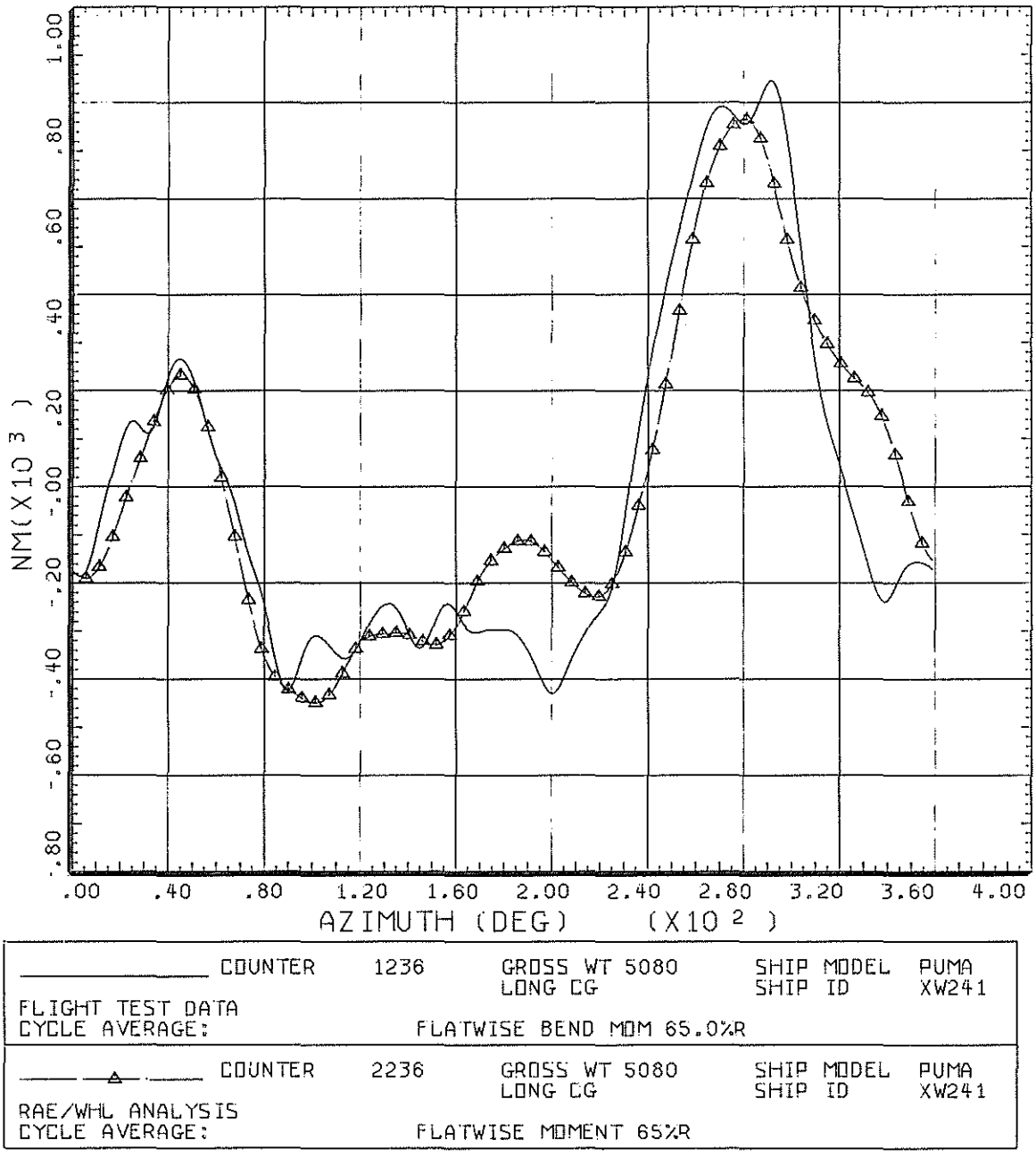

Fig 4 Measured and predicted flatwise bending moment for the Puma main rotor blade, $\mu = 0.2414$

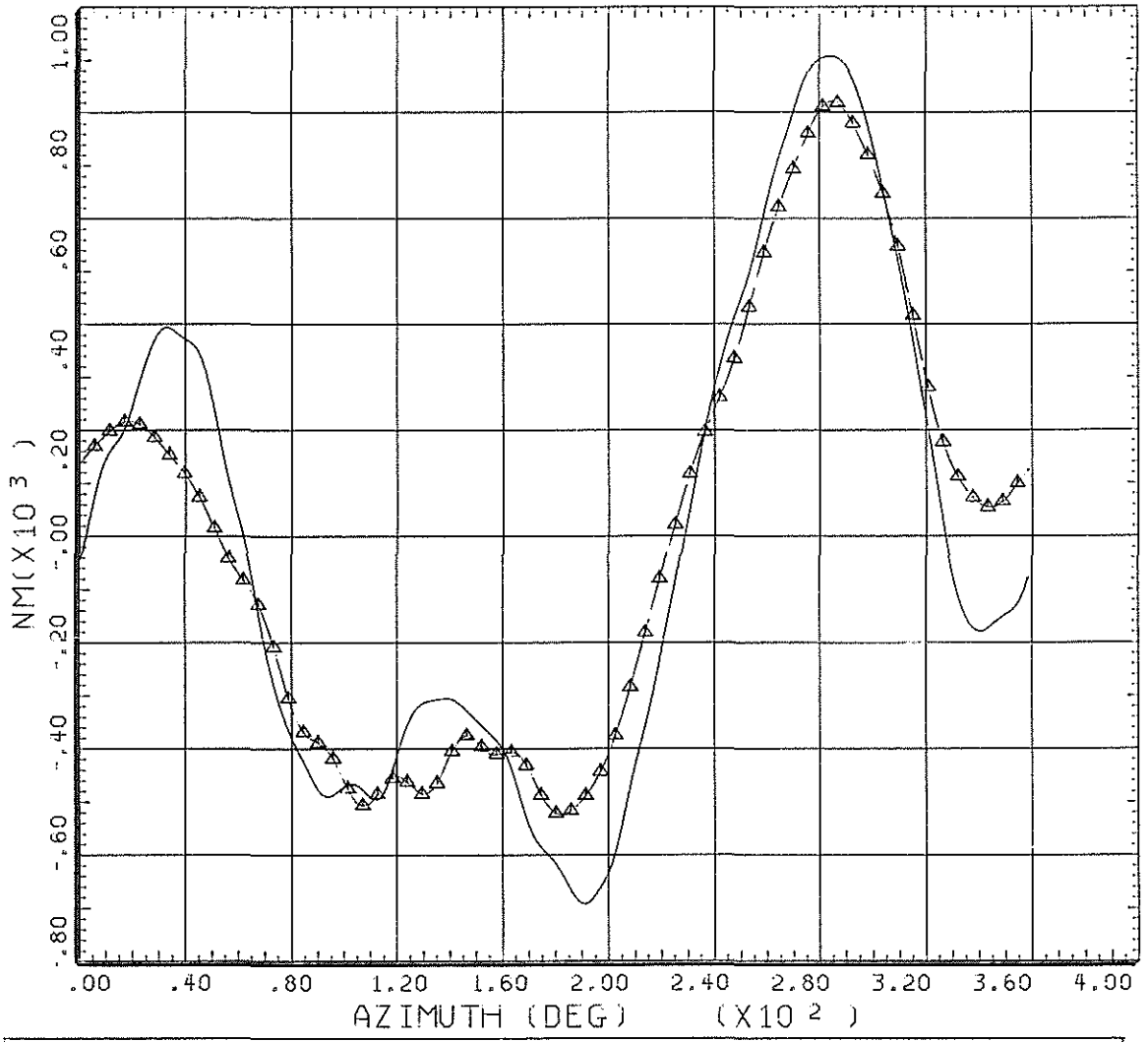

Fig 5 Measured and predicted flatwise bending moment for the Puma main rotor blade, $\mu = 0.3210$

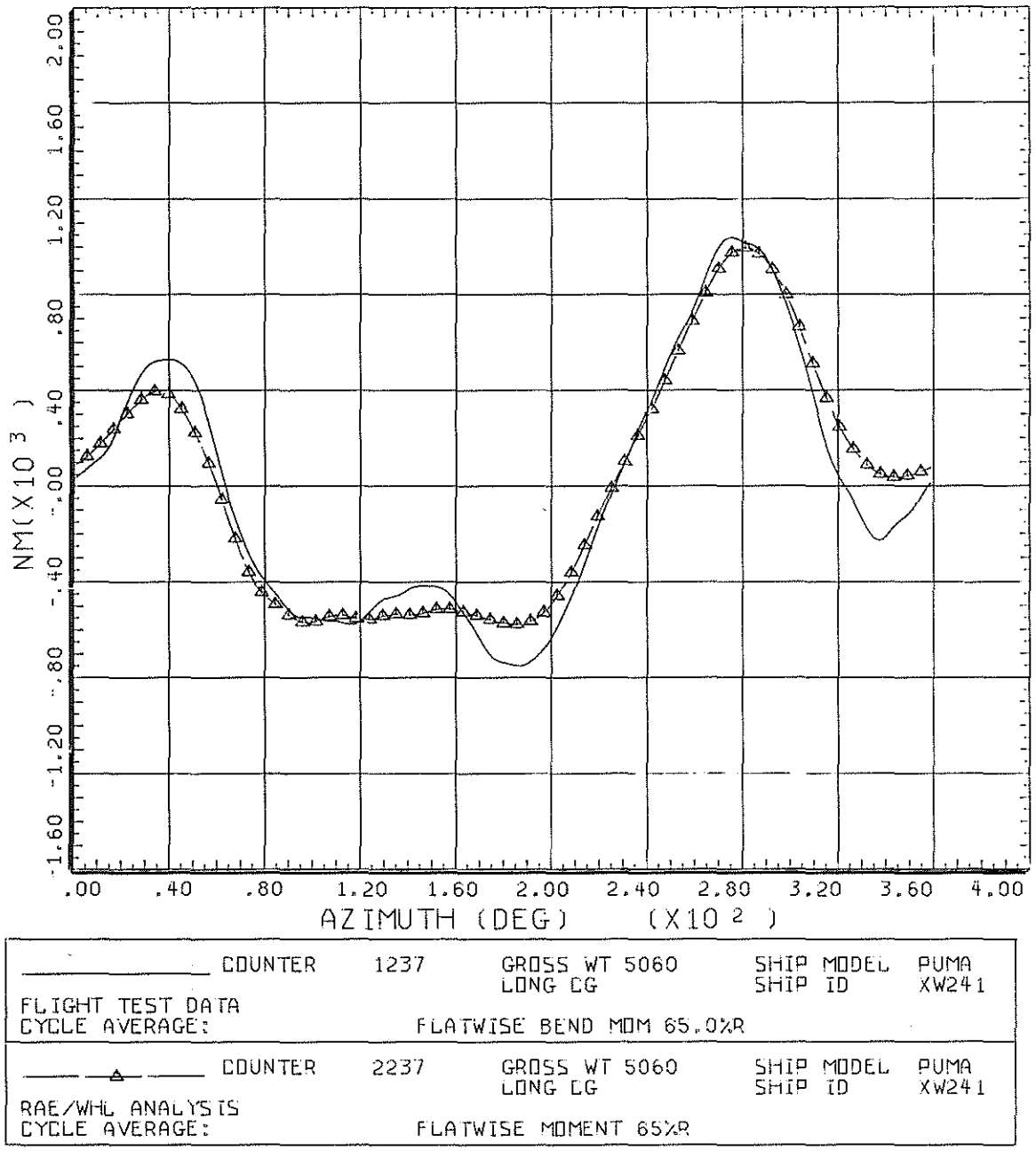

Fig 6 Measured and predicted flatwise bending moment for the Puma main rotor blade, $\mu = 0.3771$

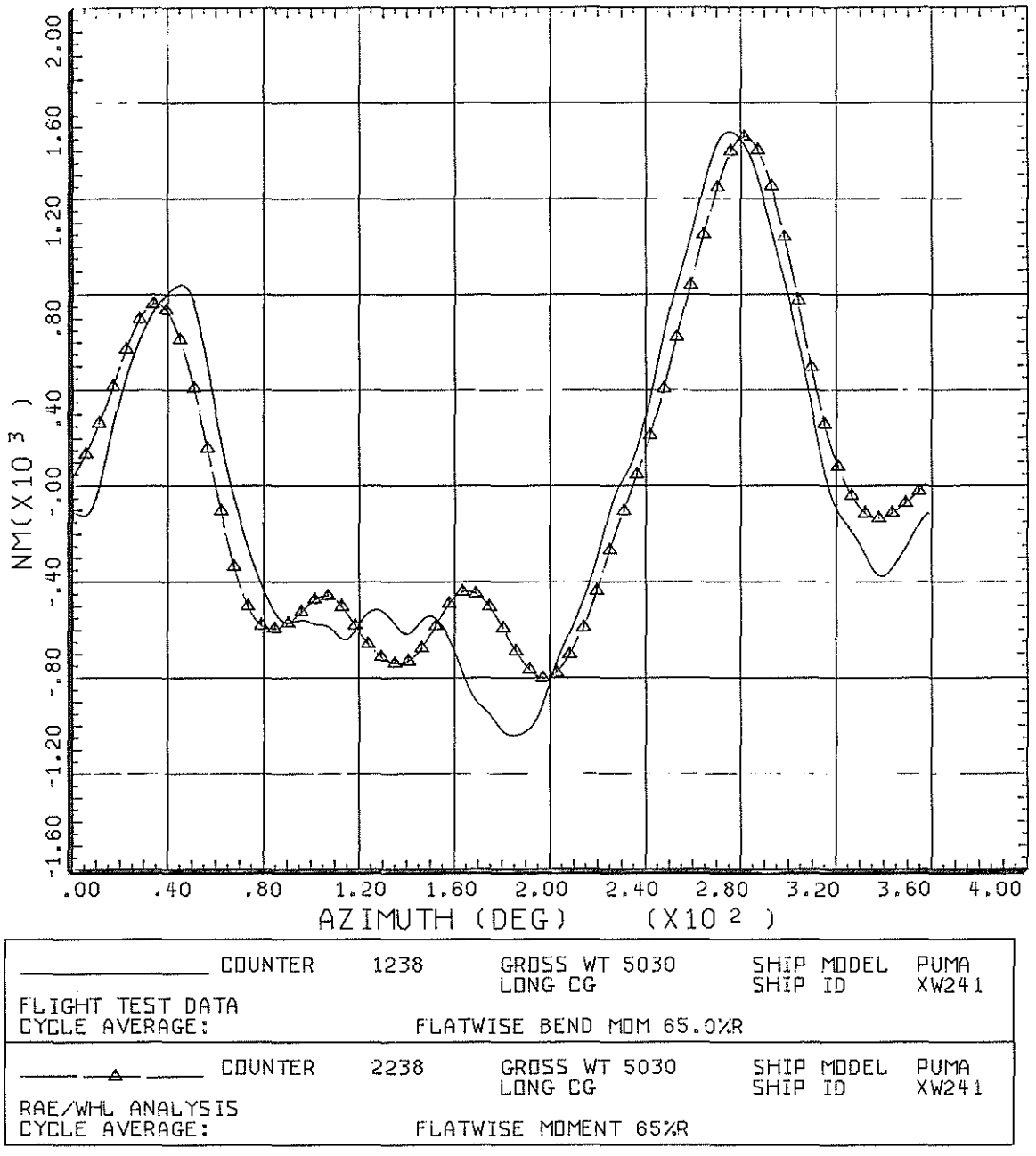

Fig 7 Measured and predicted flatwise bending moment for the Puma main rotor blade, $\mu = 0.4340$

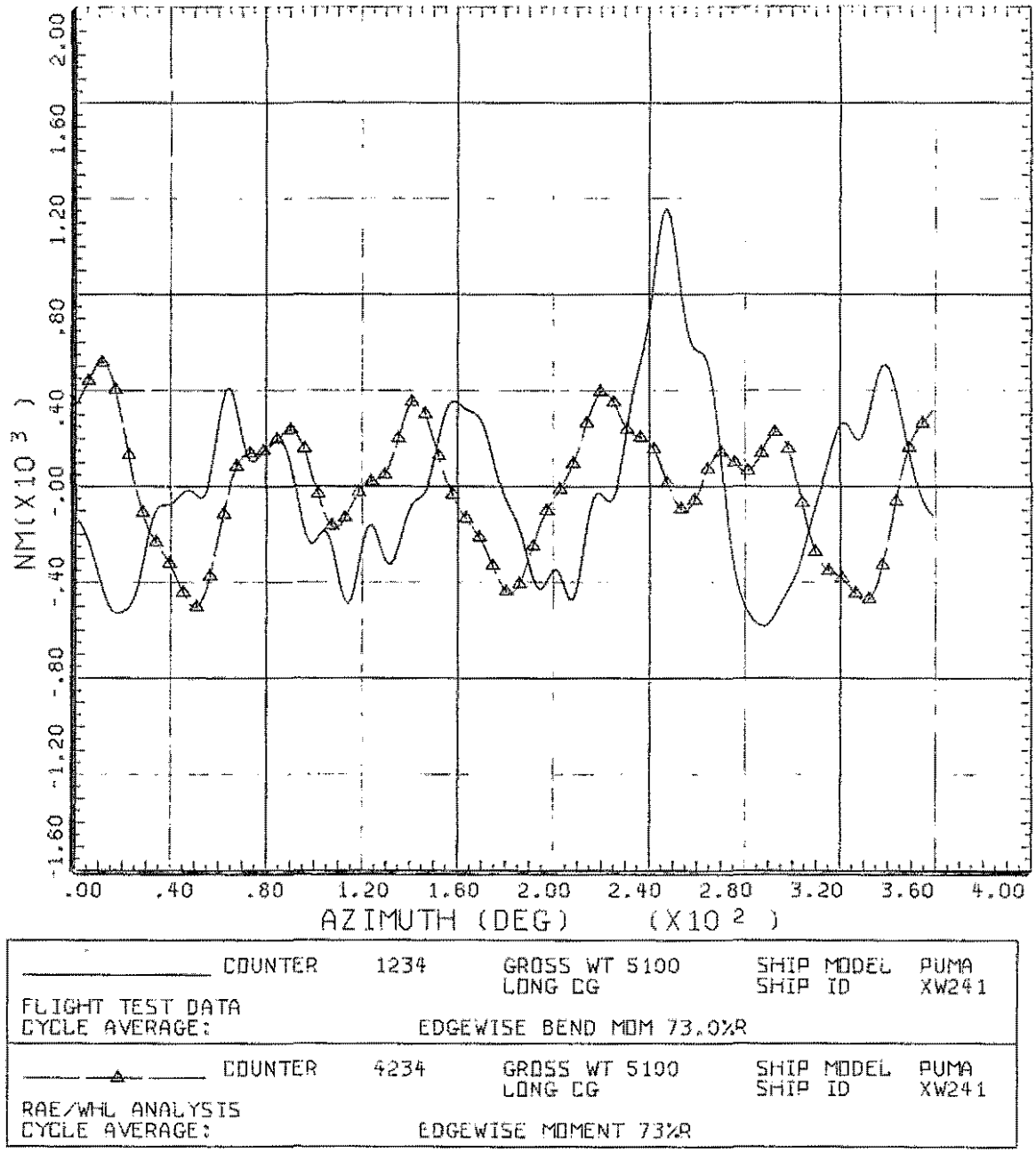

Fig 8 **Measured and predicted edgewise bending moment for the Puma main rotor blade, $\mu = 0.0972$**

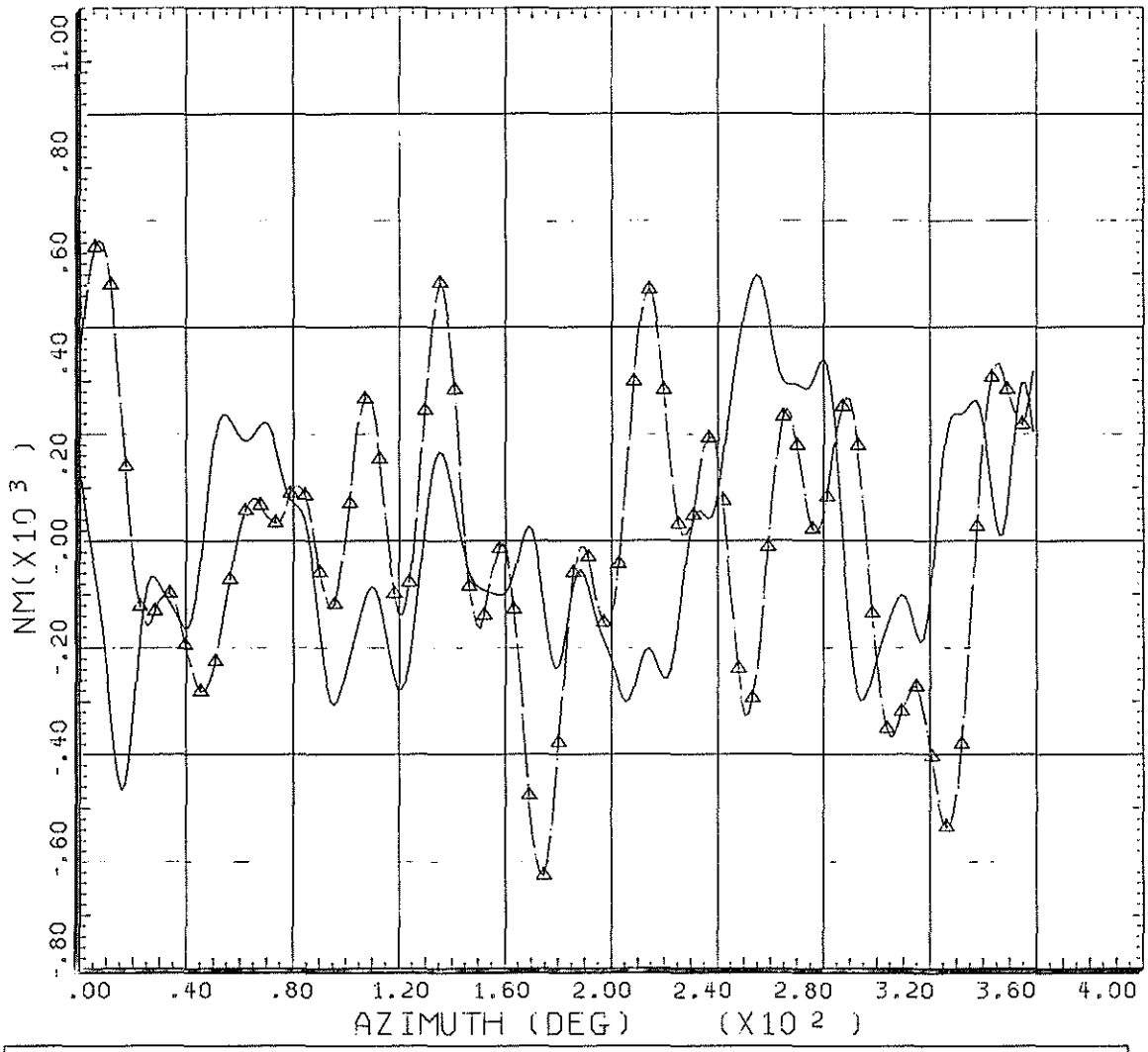

Fig 9 Measured and predicted edgewise bending moment for the Puma main rotor blade, $\mu = 0.1707$

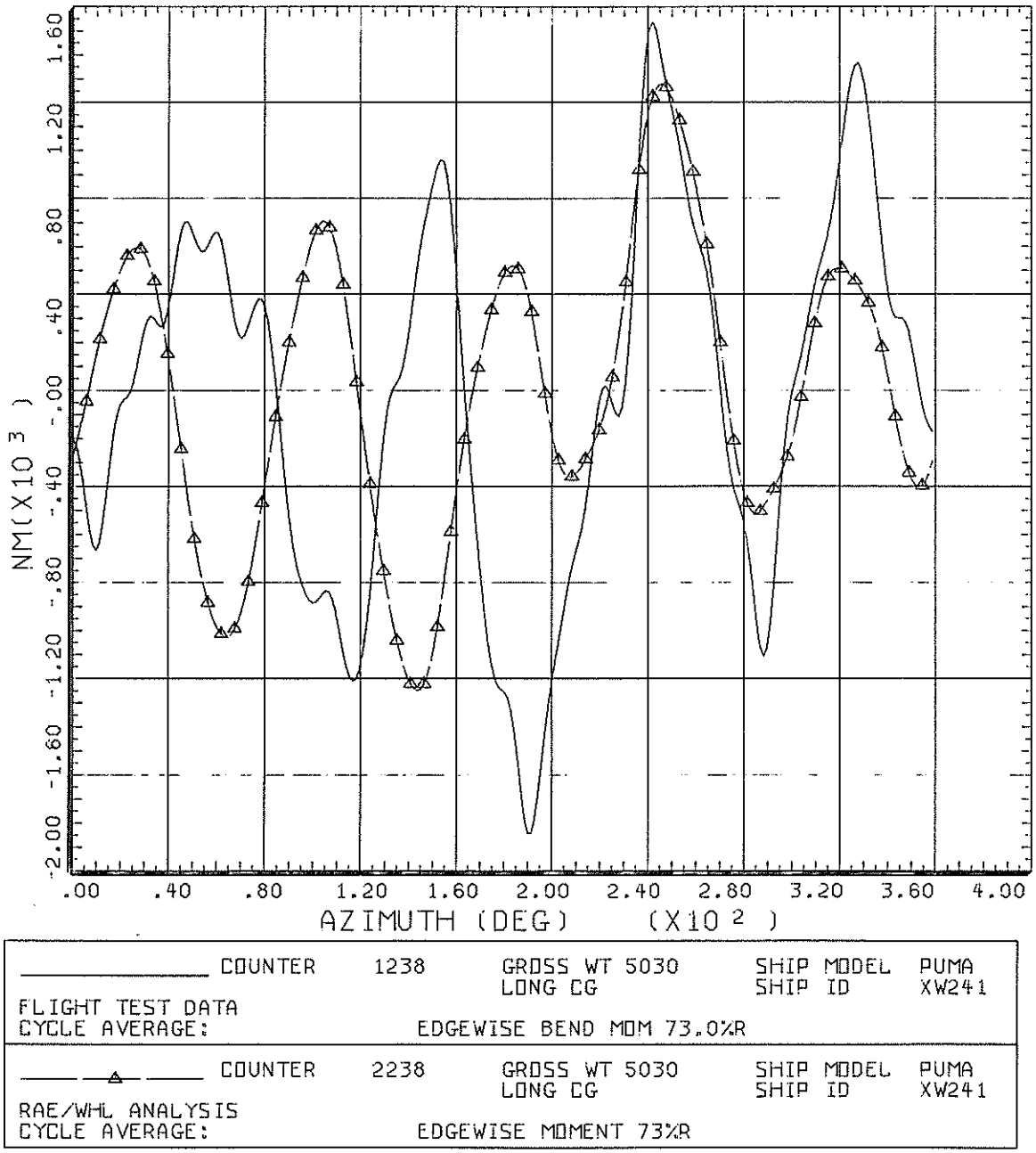

Fig 10 Measured and predicted edgewise bending moment for the Puma main rotor blade, $\mu = 0.4340$

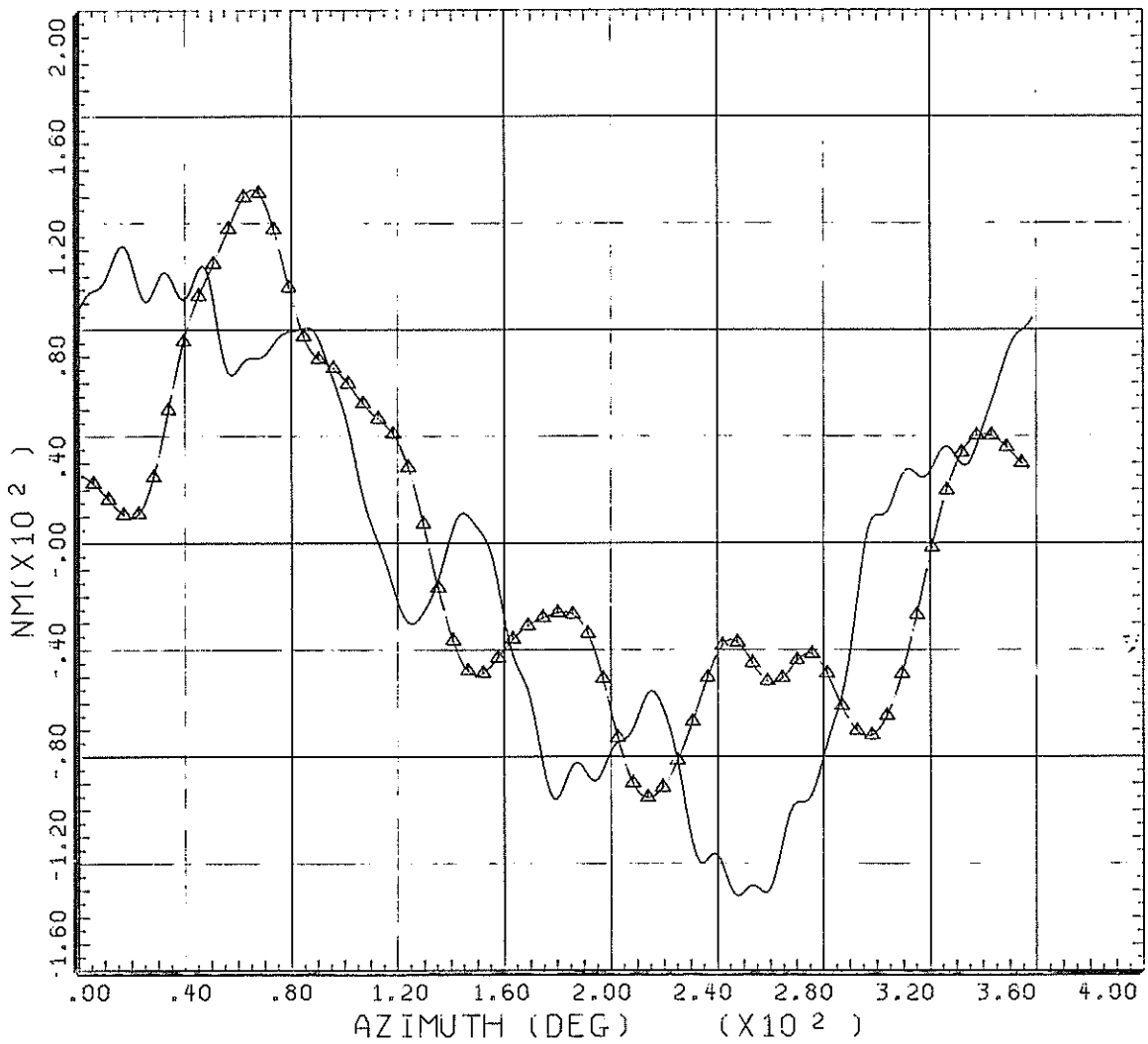

Fig 11 Measured and predicted torsion moment for the Puma main rotor blade, $\mu = 0.0972$

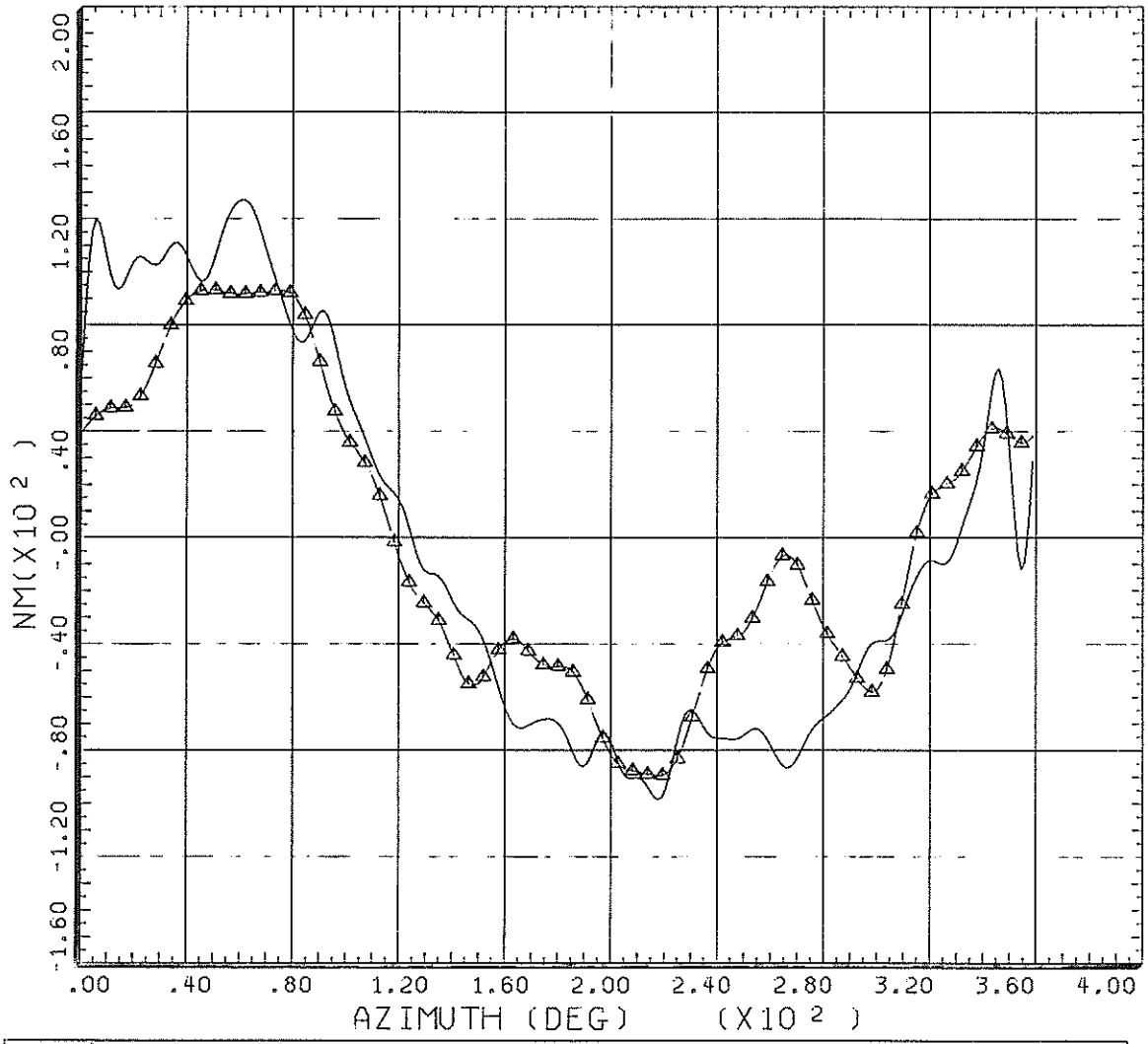

Fig 12 Measured and predicted torsion moment for the Puma main rotor blade, $\mu = 0.1707$

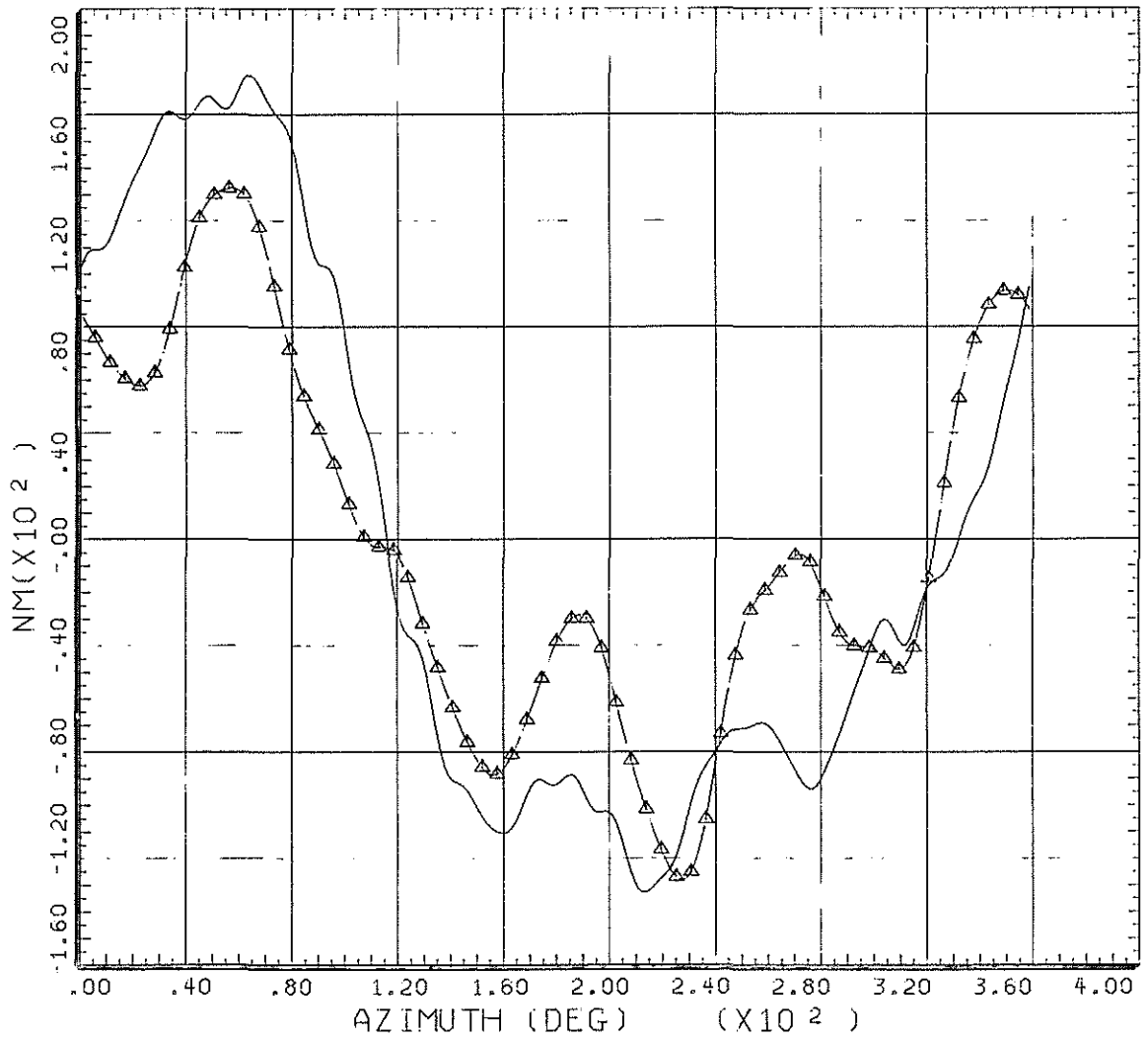

Fig 13 Measured and predicted torsion moment for the Puma main rotor blade, $\mu = 0.2414$

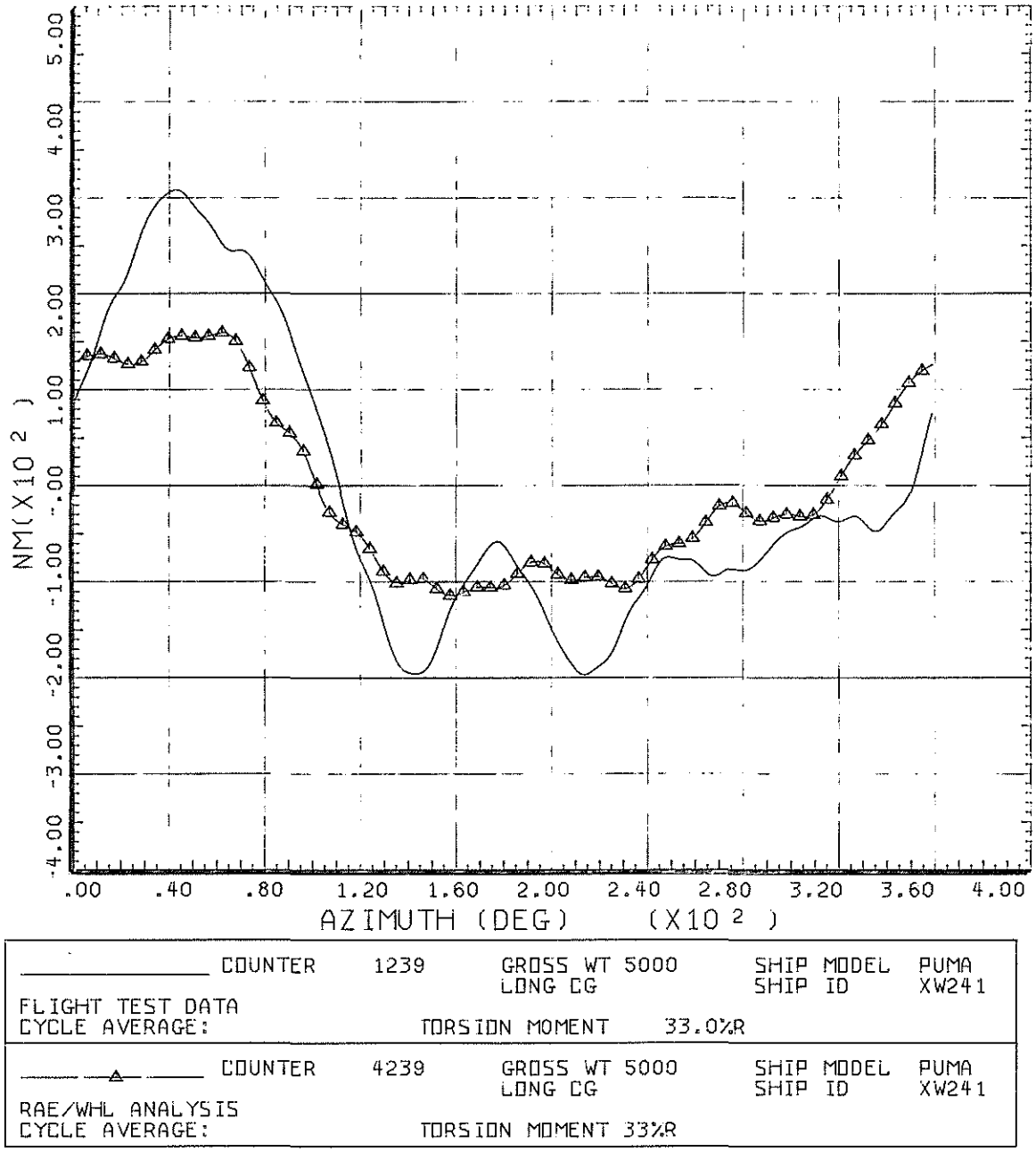

Fig 14 Measured and predicted torsion moment for the Puma main rotor blade, $\mu = 0.3210$

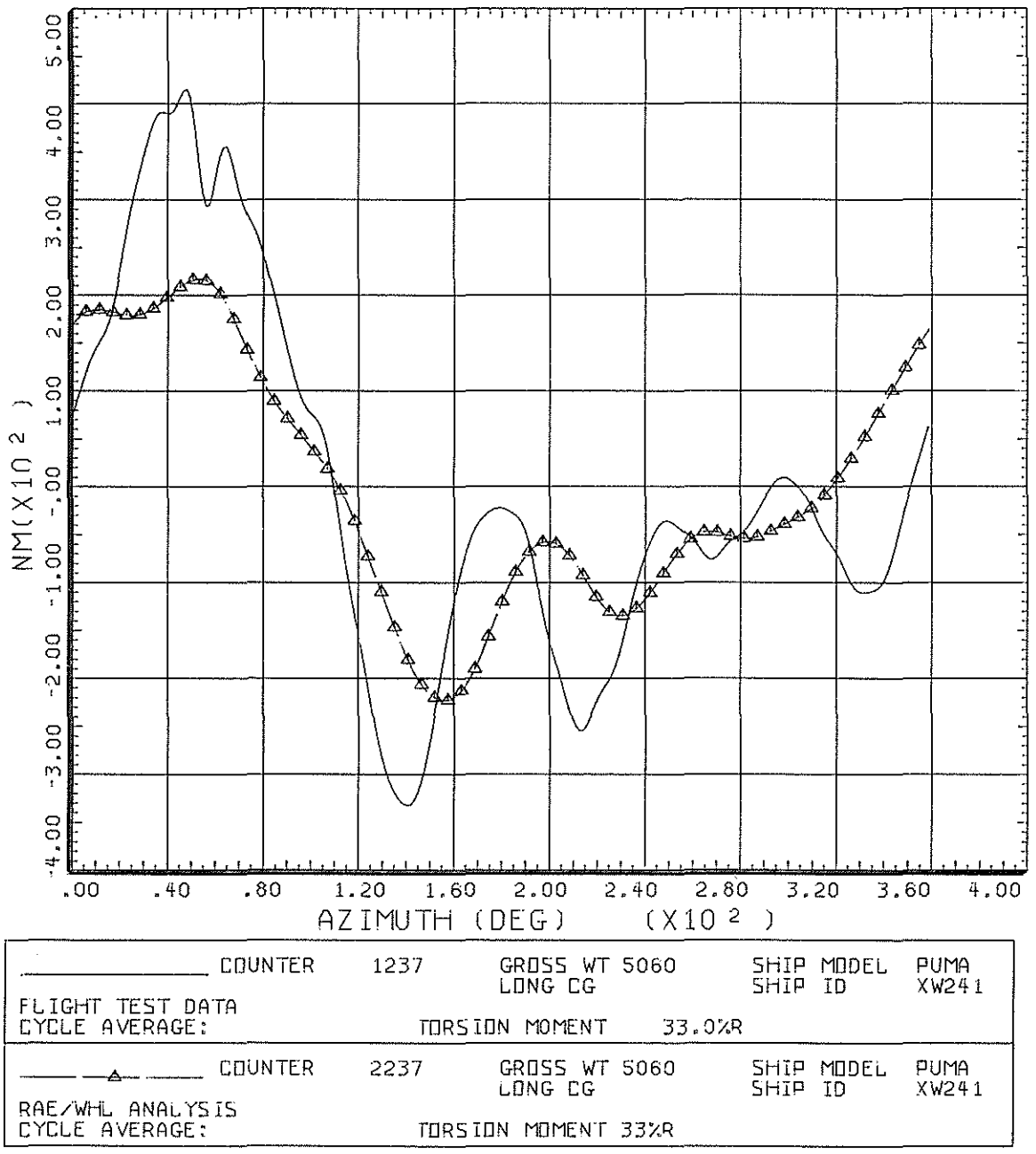

Fig 15 Measured and predicted torsion moment for the Puma main rotor blade, $\mu = 0.3771$

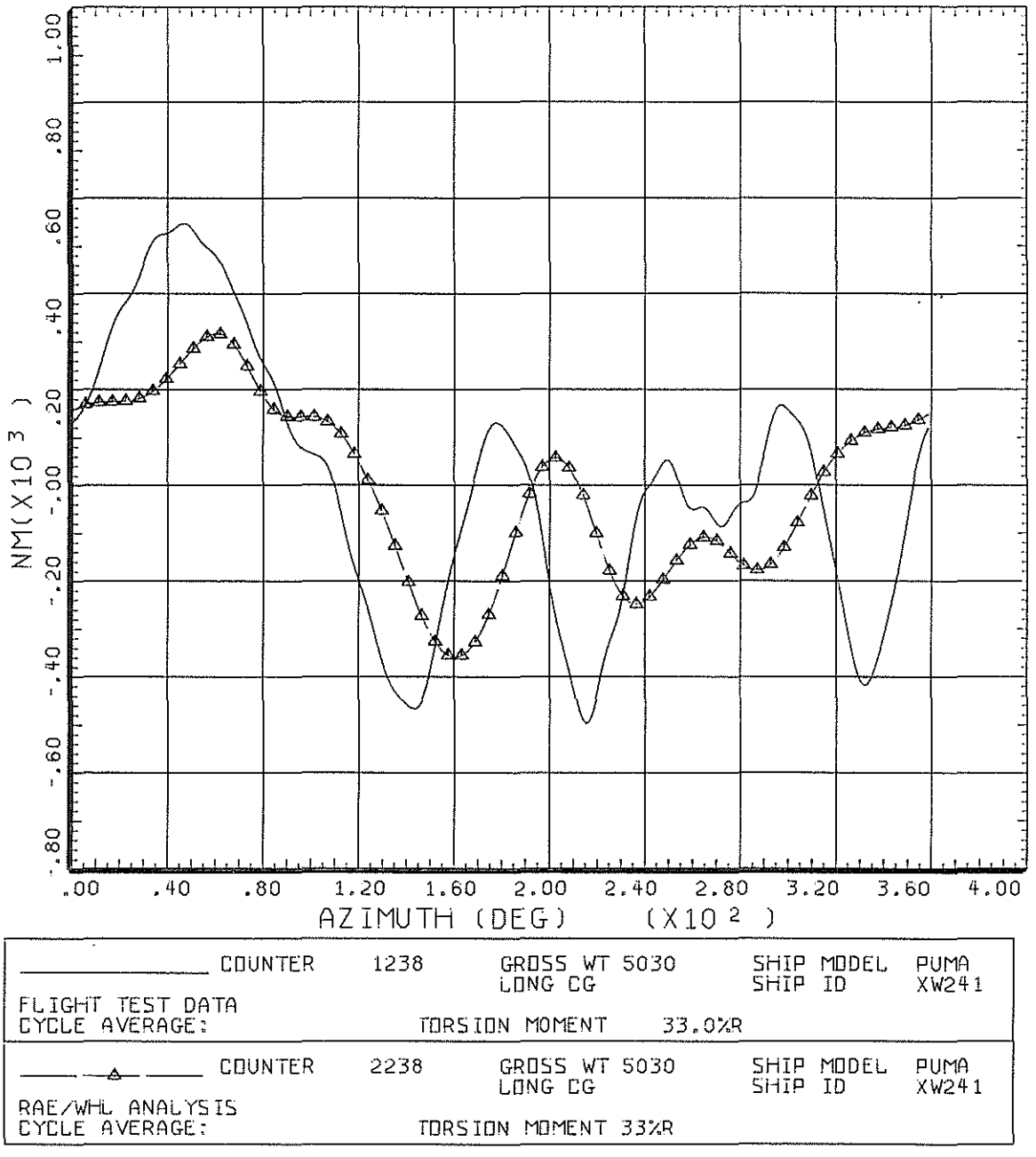

Fig 16 Measured and predicted torsion moment for the Puma main rotor blade, $\mu = 0.4340$

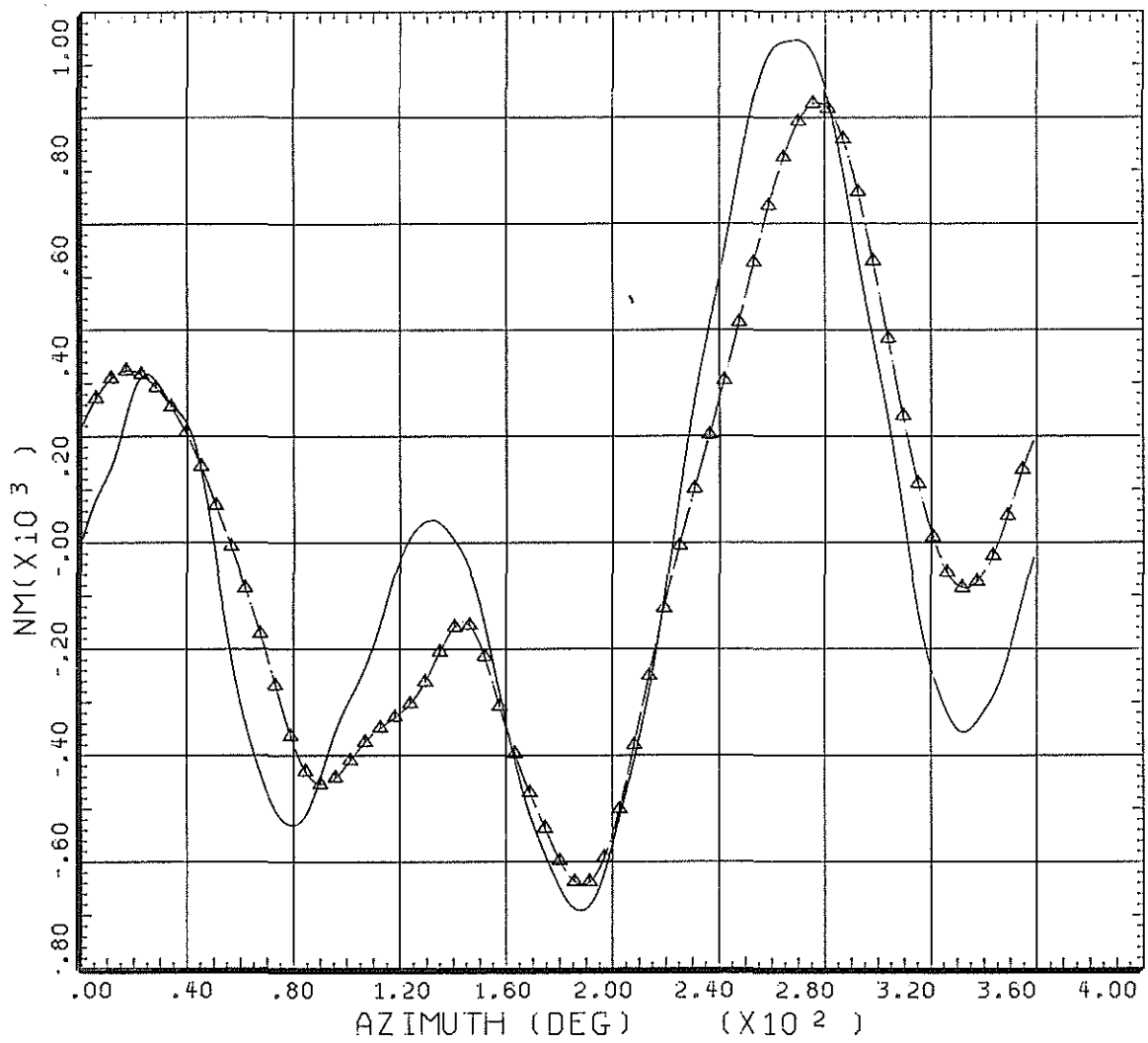

Fig 17 Measured and predicted flatwise bending moment for the swept tip Puma blade

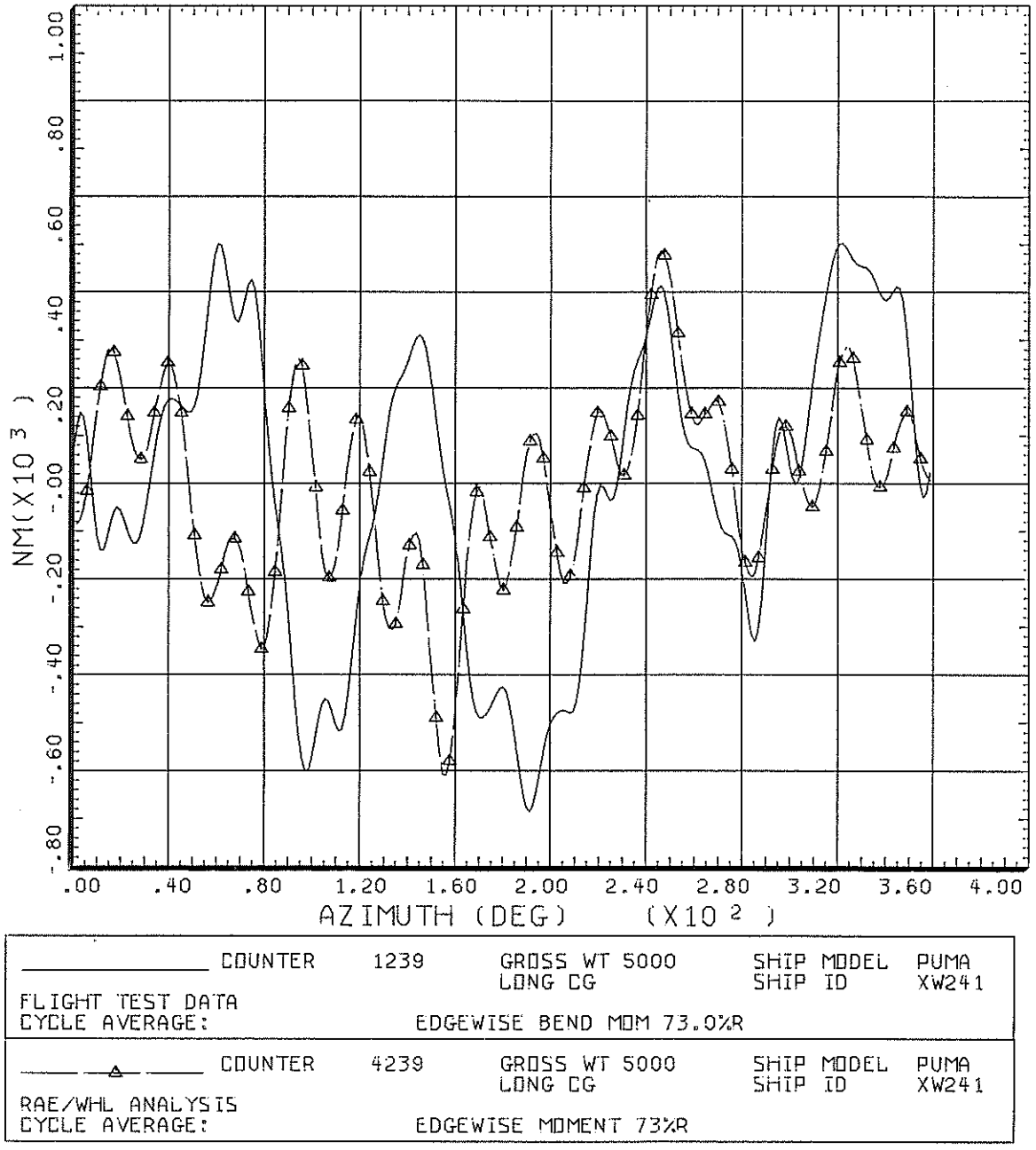

Fig 18 Measured and predicted edgewise bending moment for the standard Puma blade

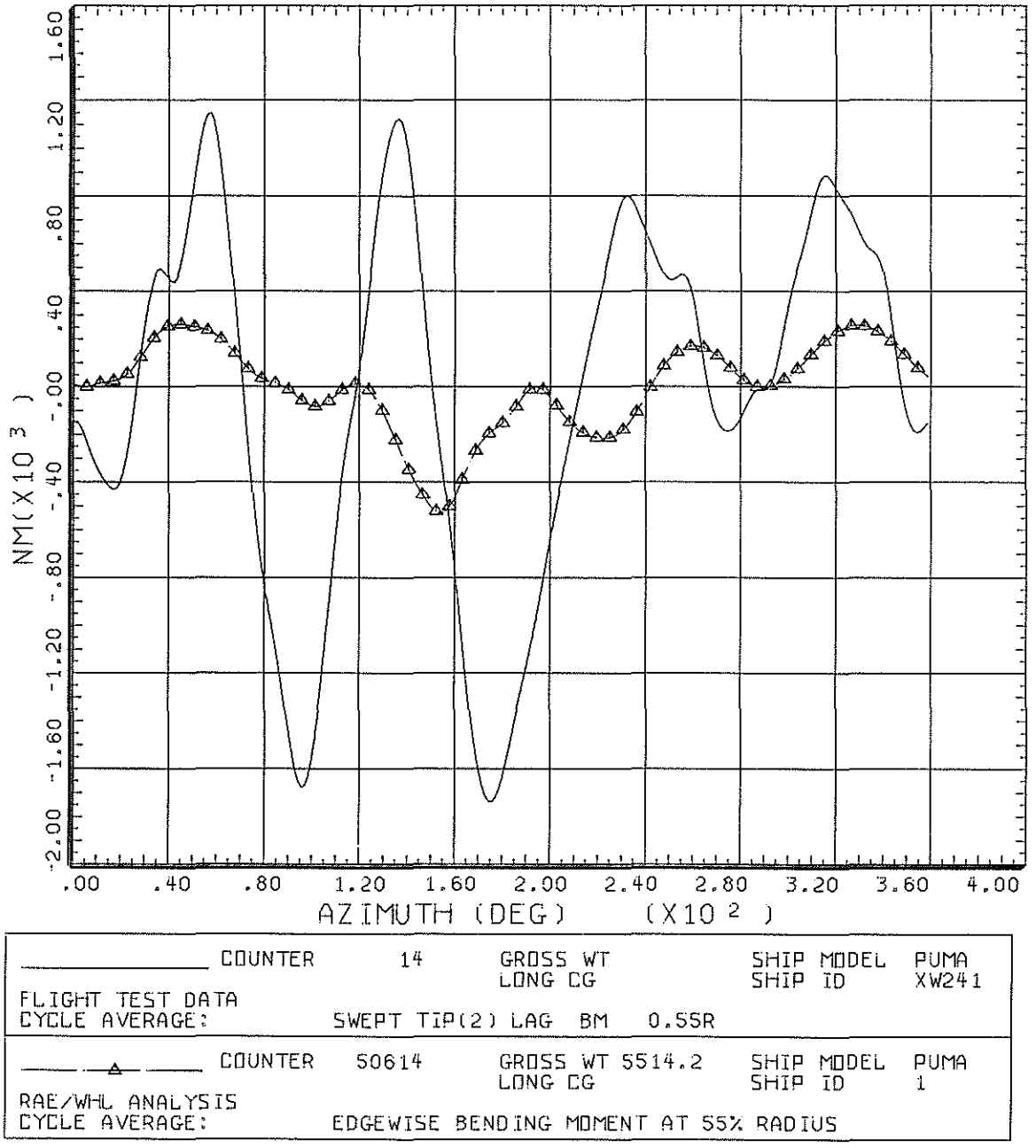

Fig 19 Measured and predicted edgewise bending moment for the swept tip Puma blade

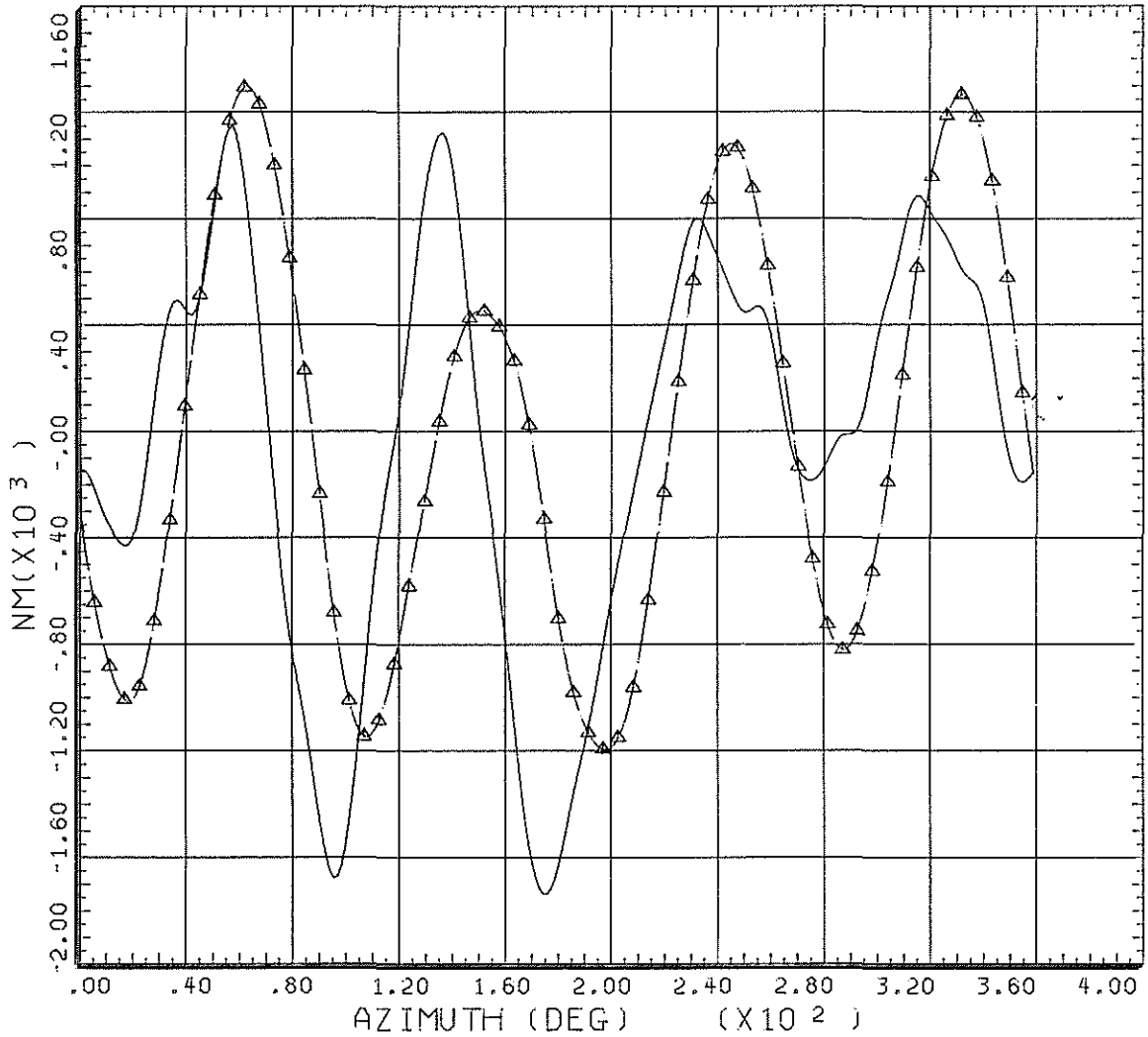

Fig 20 Effect of reducing the lag mode frequency on the edgewise bending moment for the swept tip blade

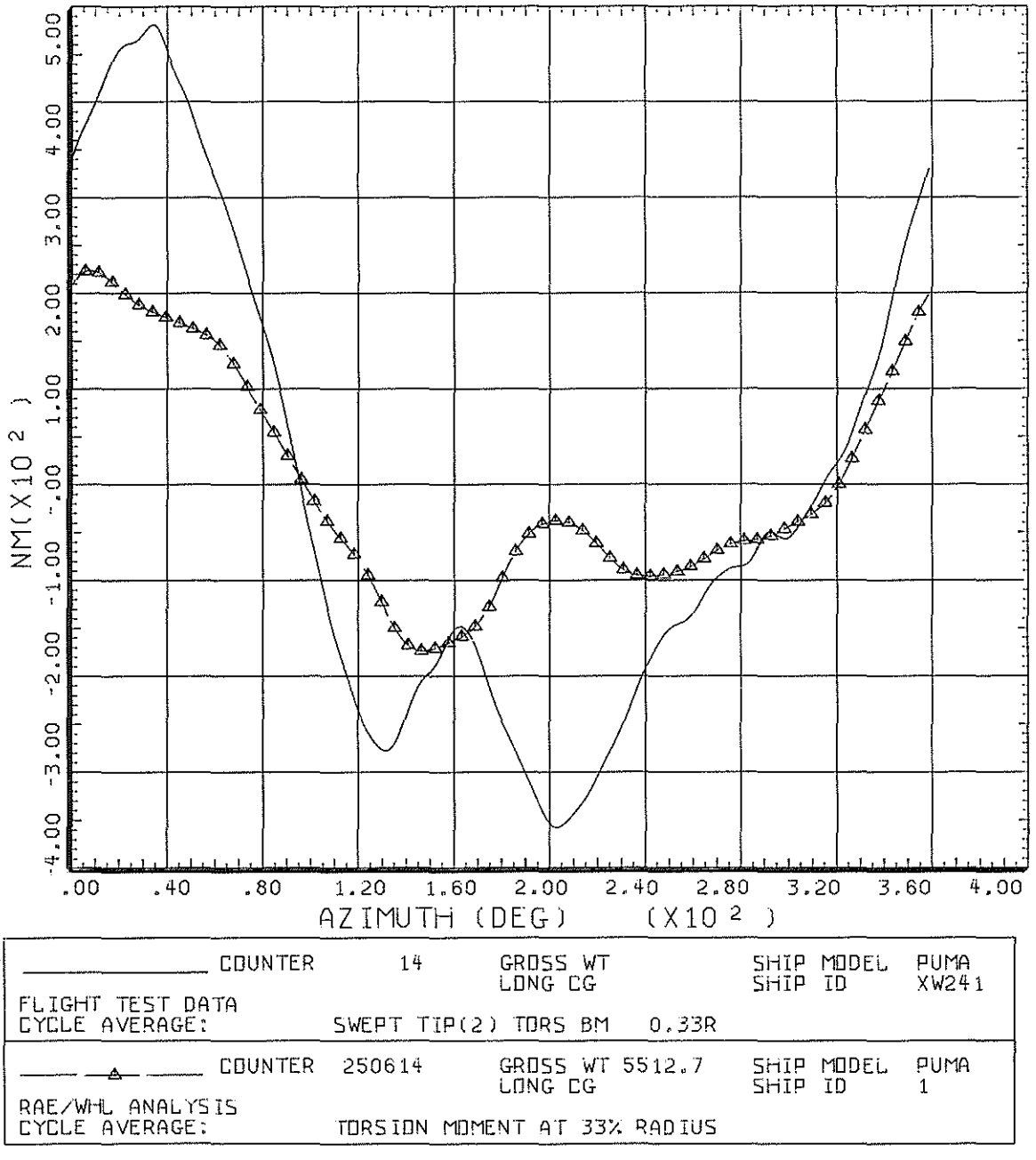

Fig 21 Measured and predicted torsion moment for the swept tip Puma blade

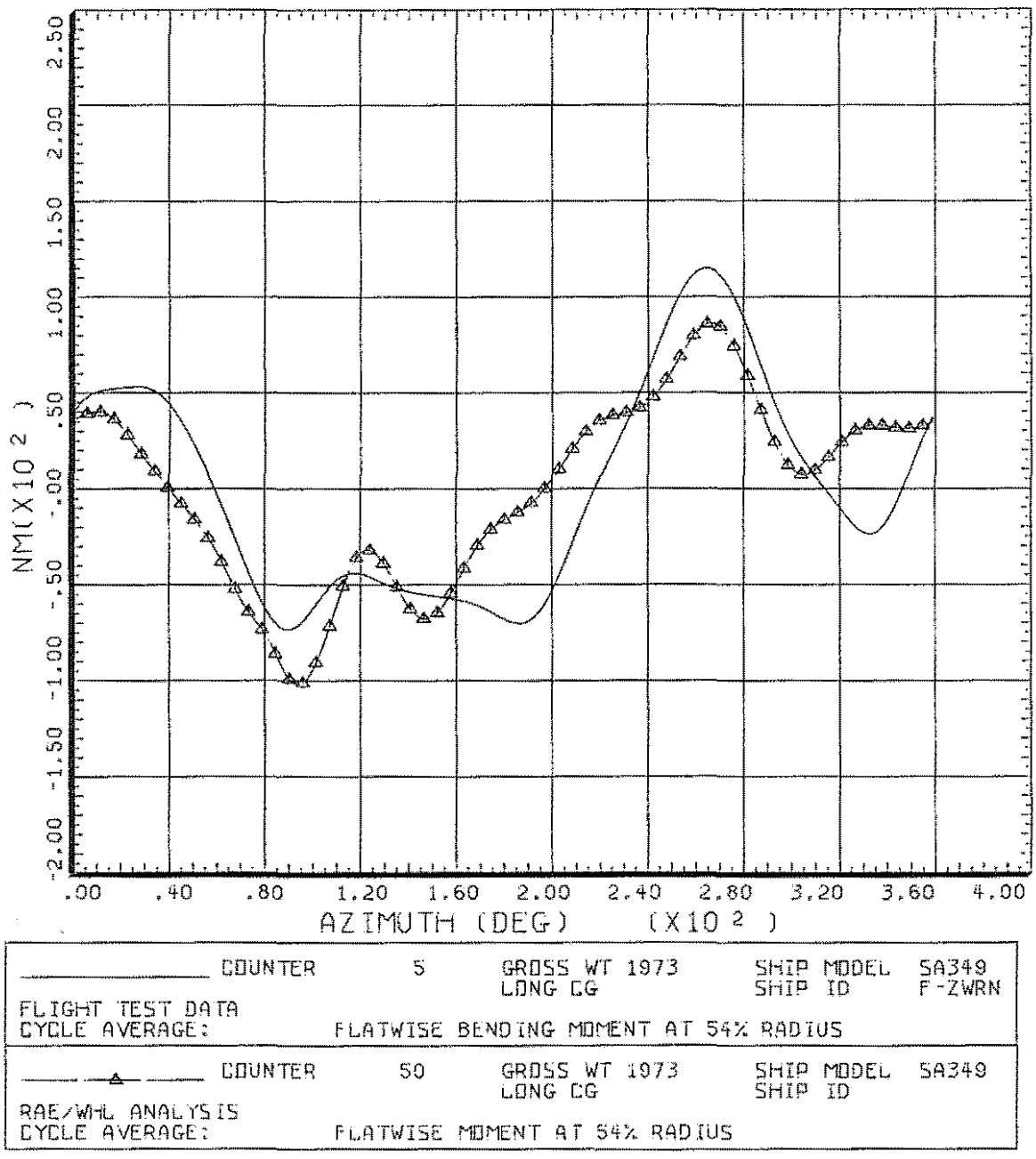

Fig 22 Measured and predicted flatwise bending moment for the SA349 main rotor blade

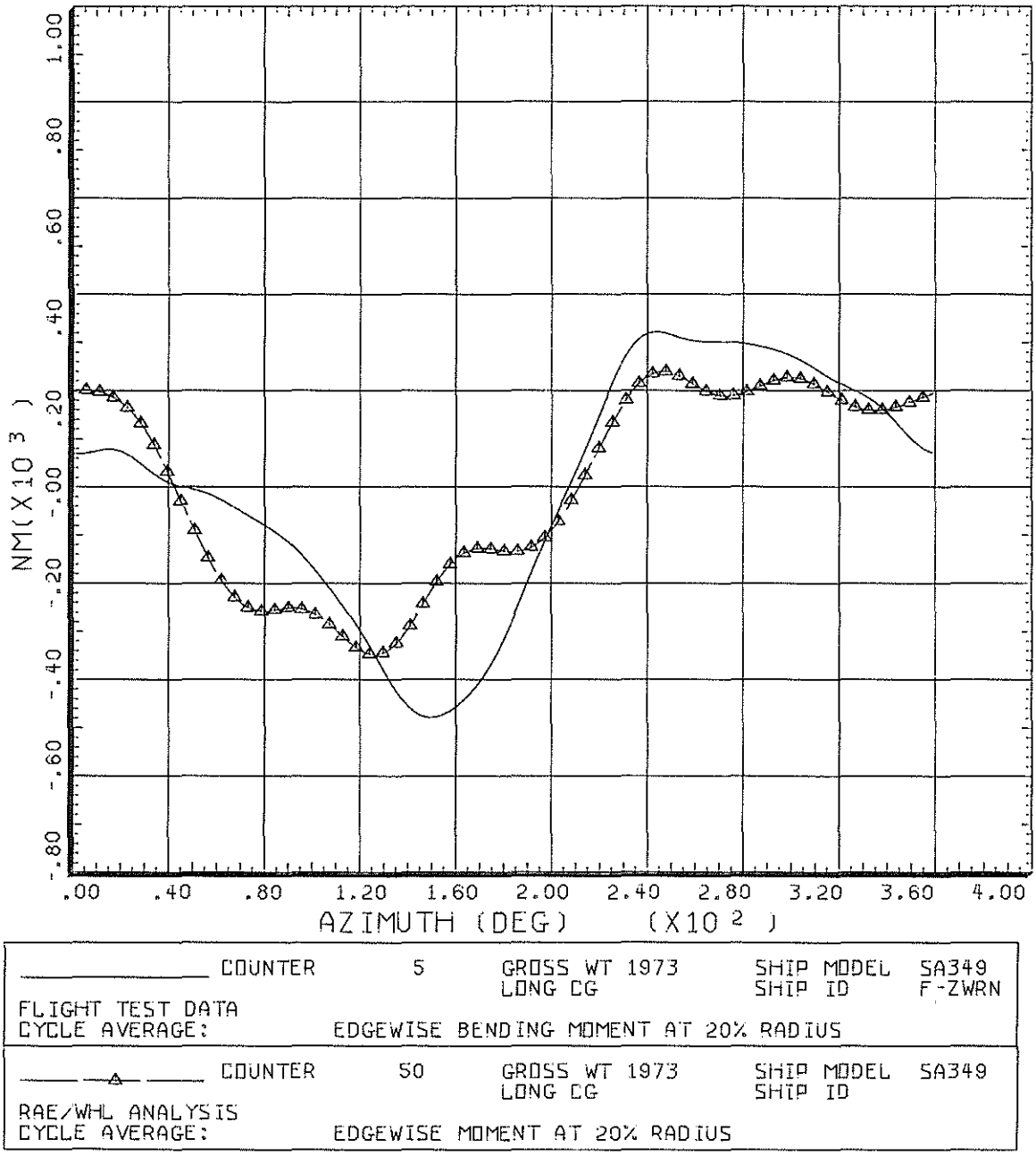

Fig 23 Measured and predicted edgewise bending moment at 20% radius for the SA349 main rotor blade

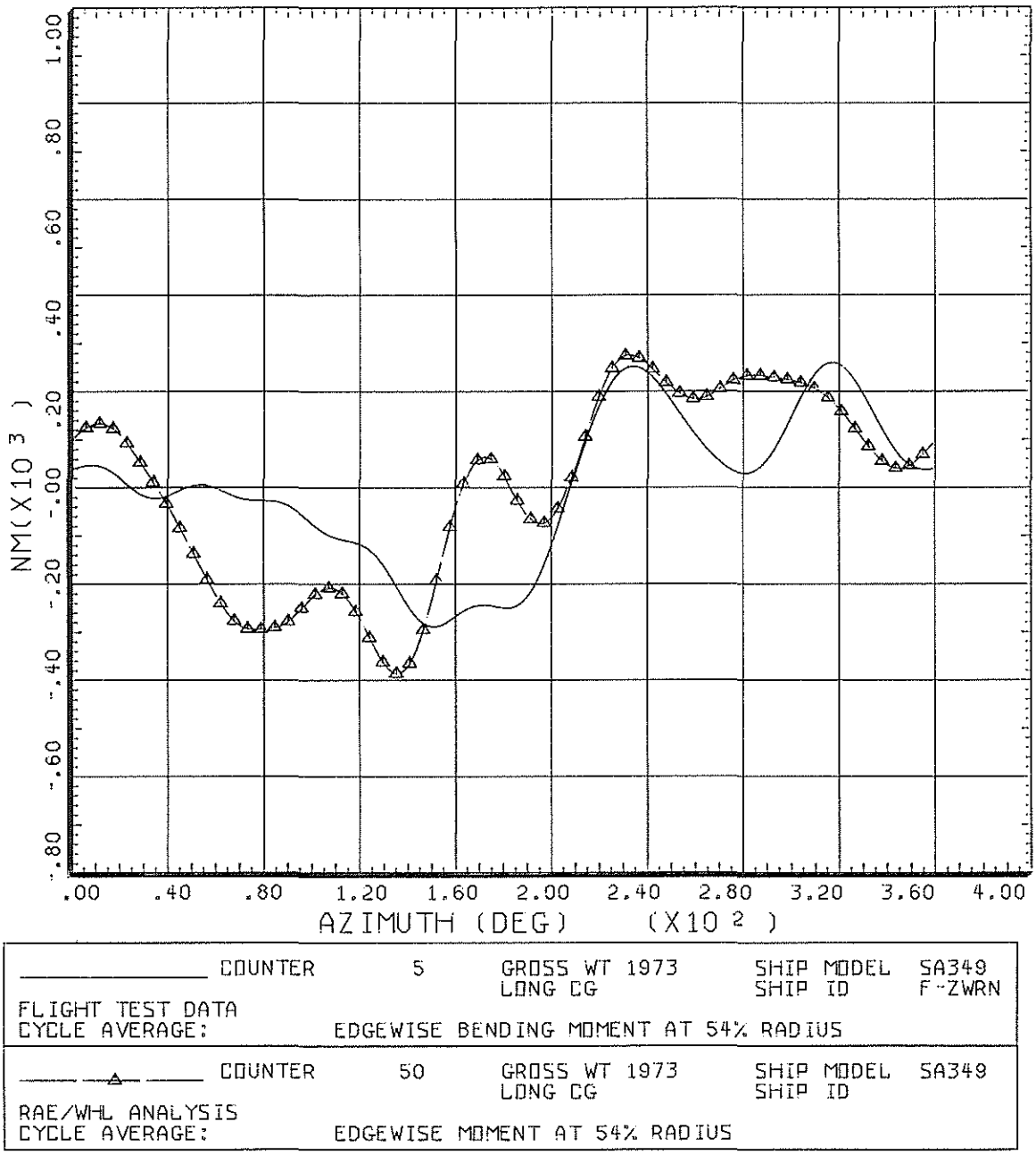

Fig 24 Measured and predicted edgewise bending moment at 54% radius for the SA349 main rotor blade

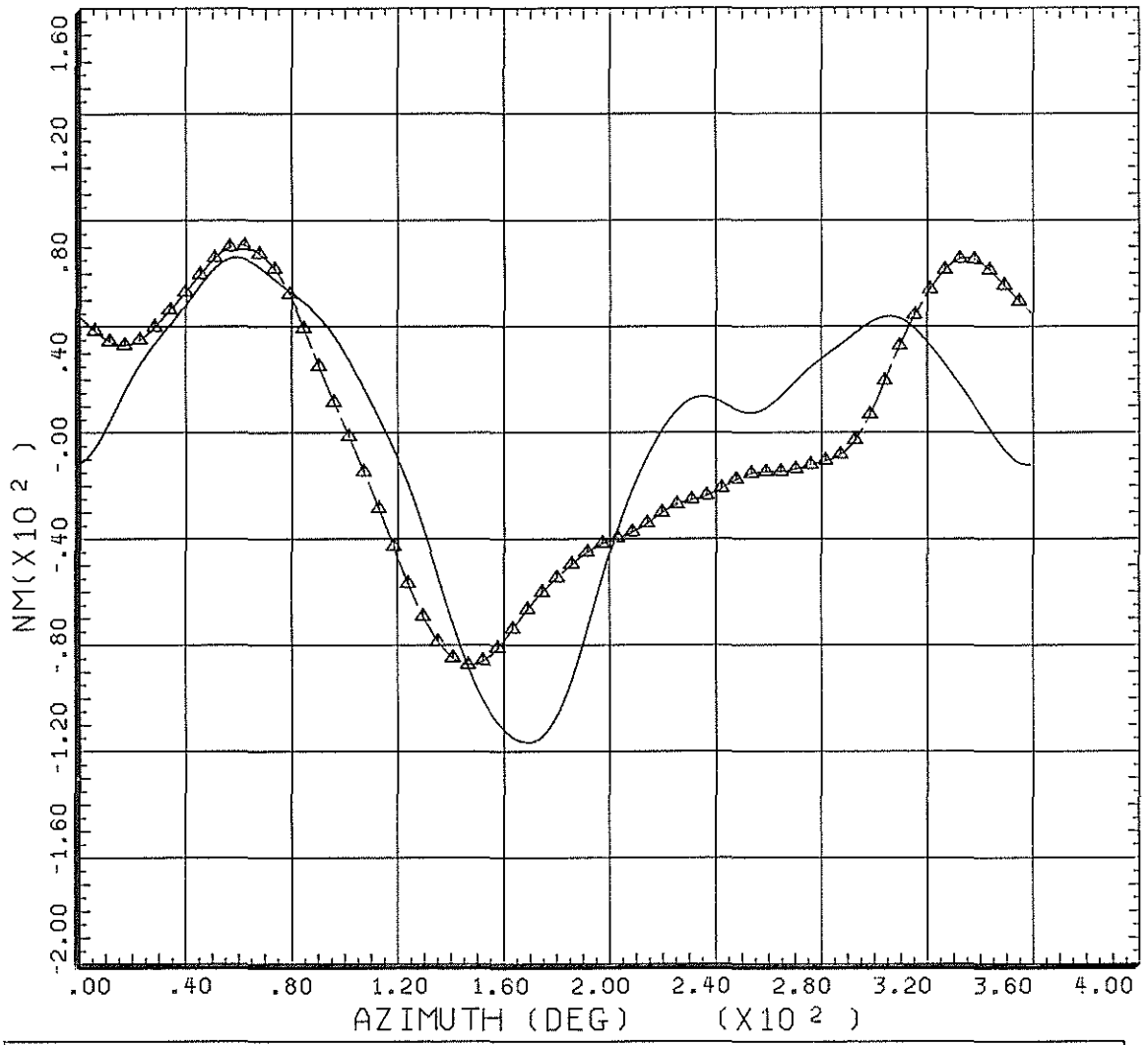

Fig 25 Measured and predicted torsion moment for the SA349 main rotor blade

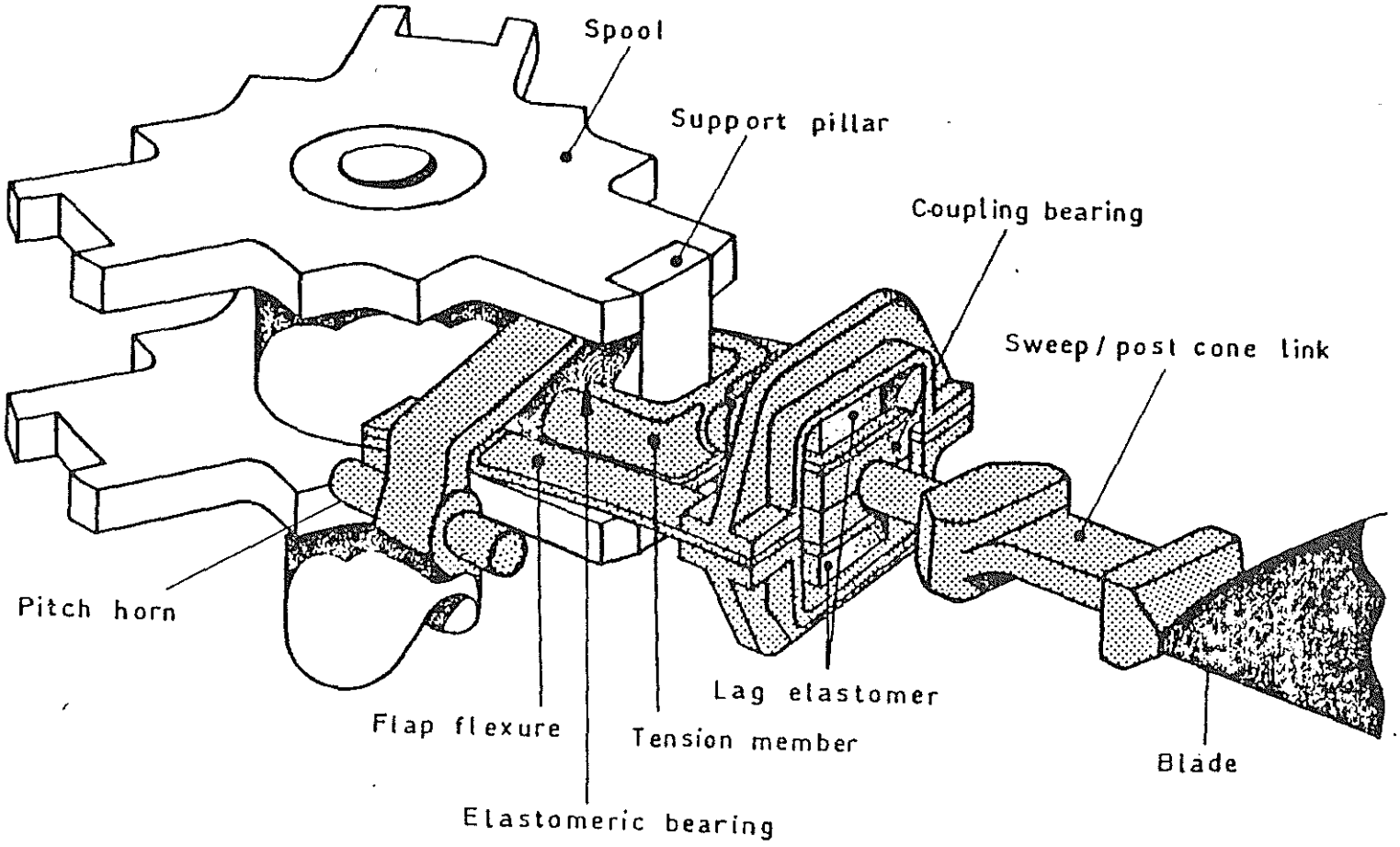

Fig 26 Sketch of the split load path model rotor

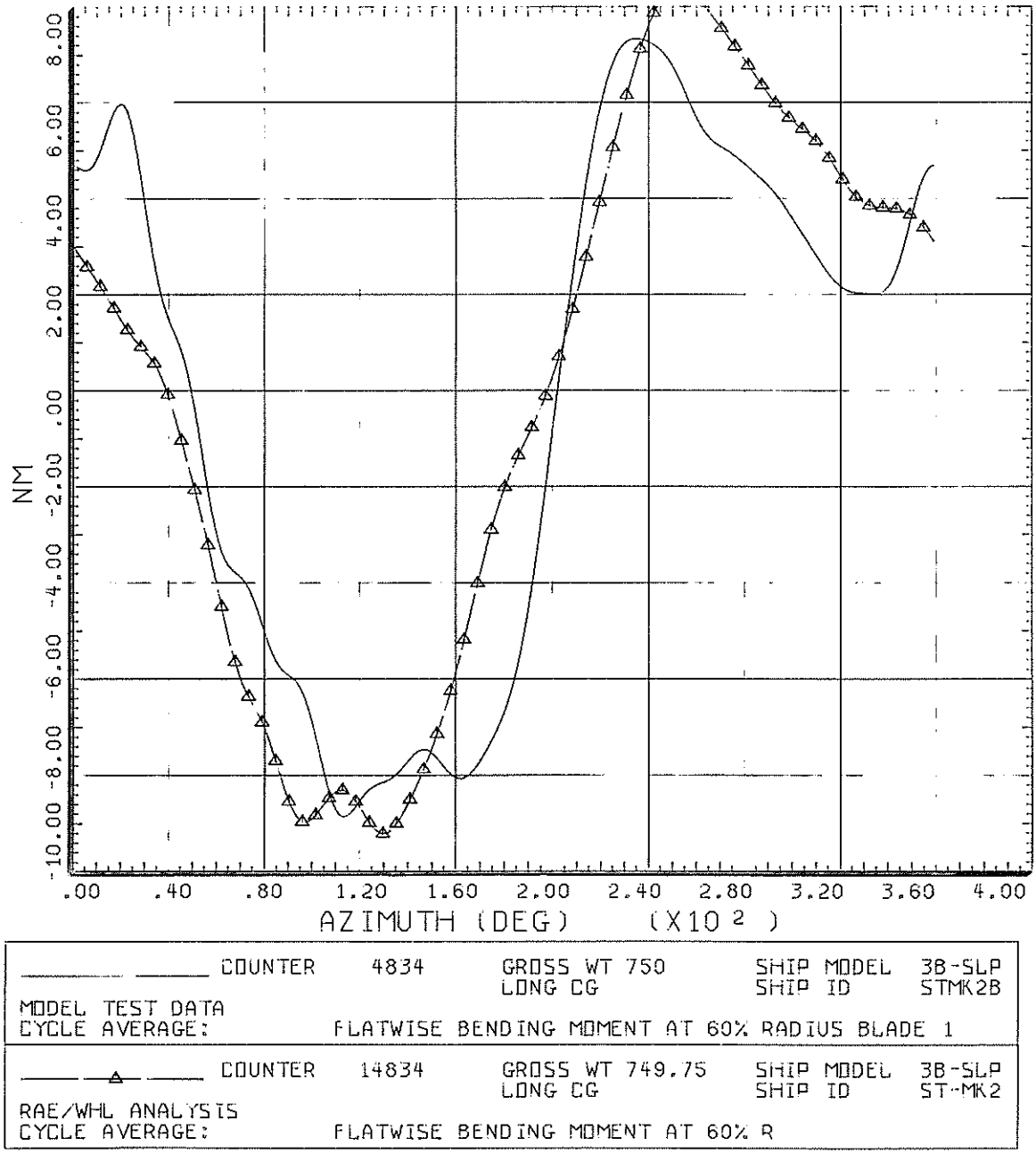

Fig 27 Measured and predicted flatwise bending moment for the model rotor with straight blades

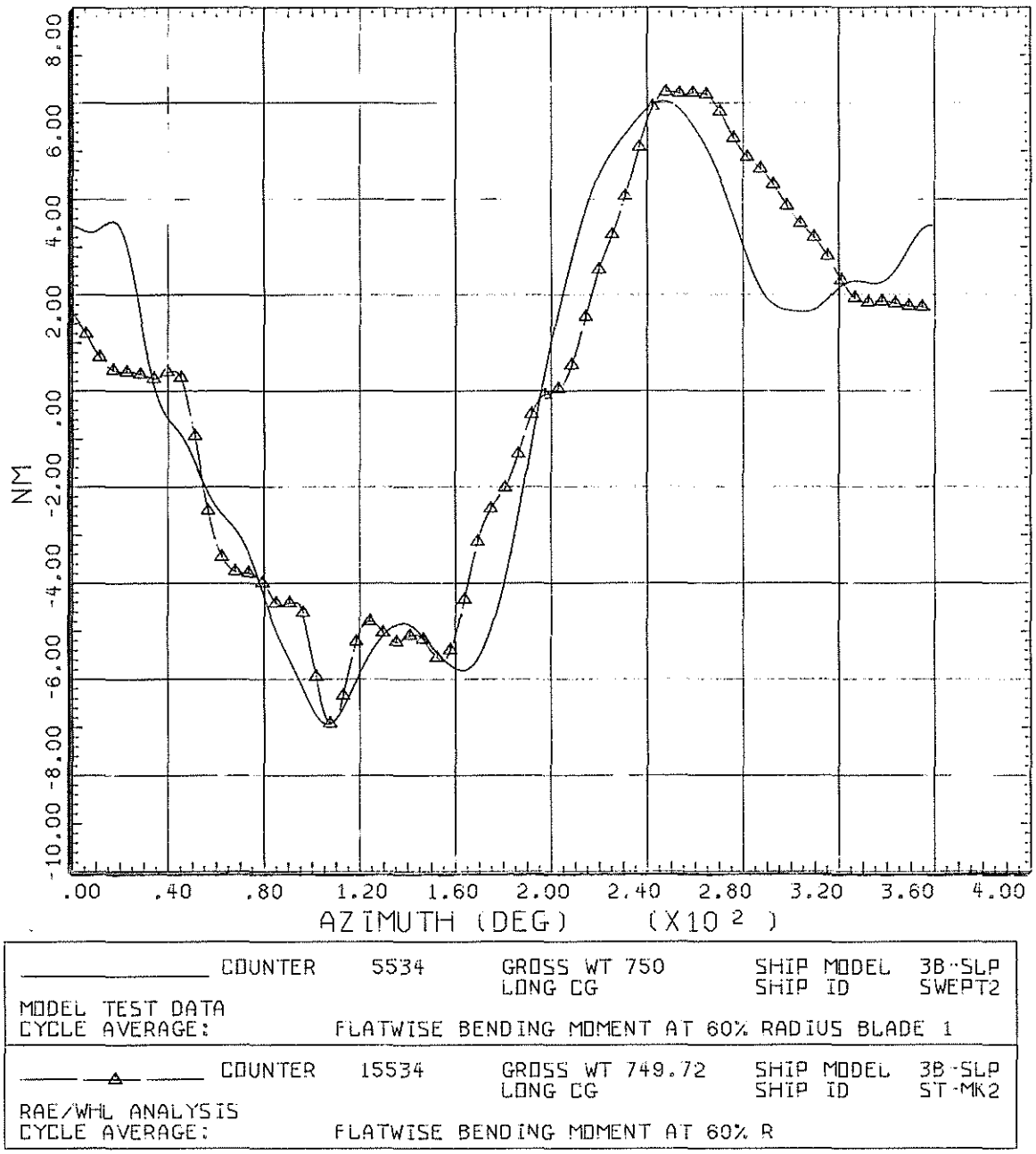

Fig 28 Measured and predicted flatwise bending moment for the model rotor with swept tip blades

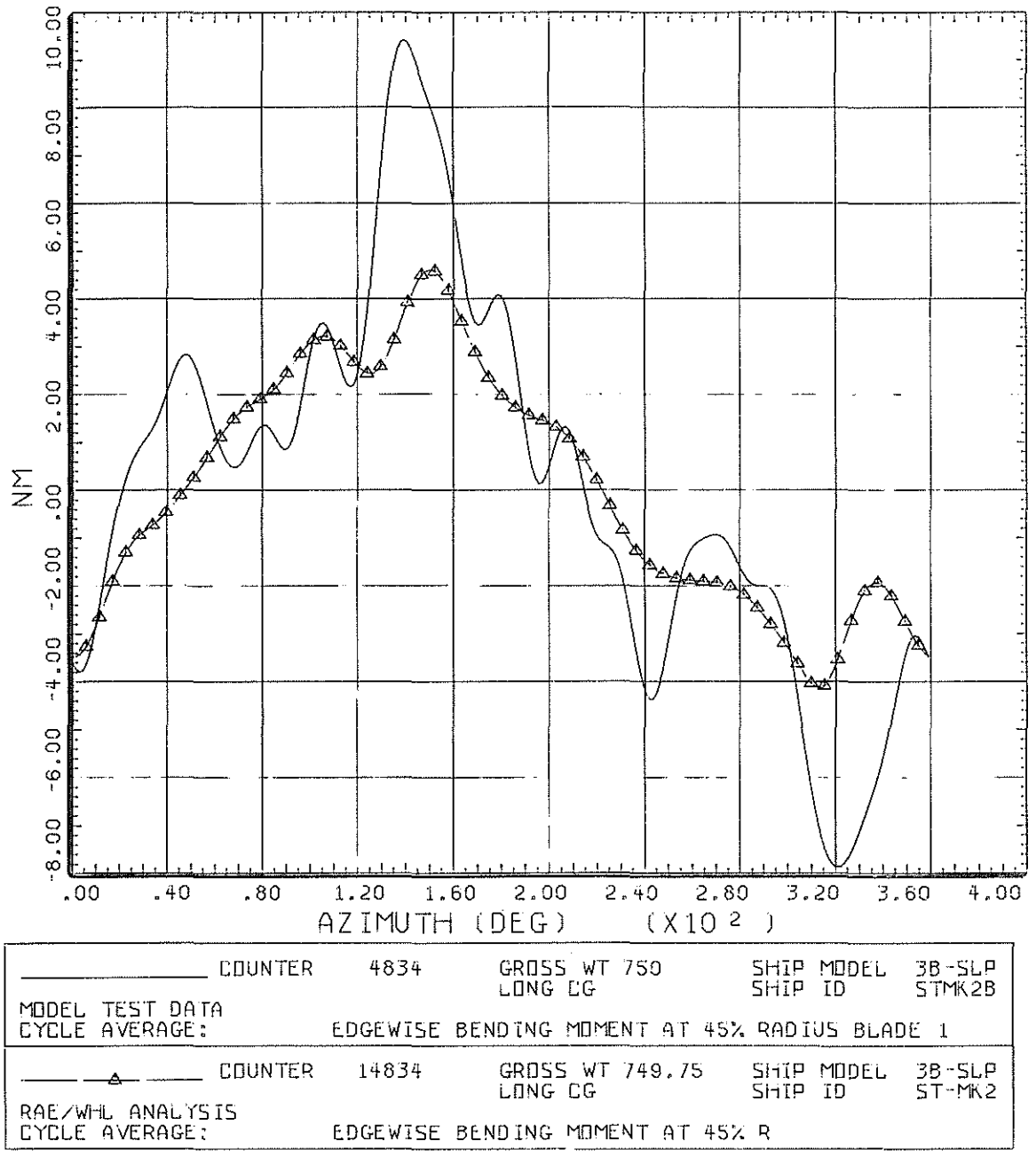

Fig 29 Measured and predicted edgewise bending moment for the model rotor with straight blades

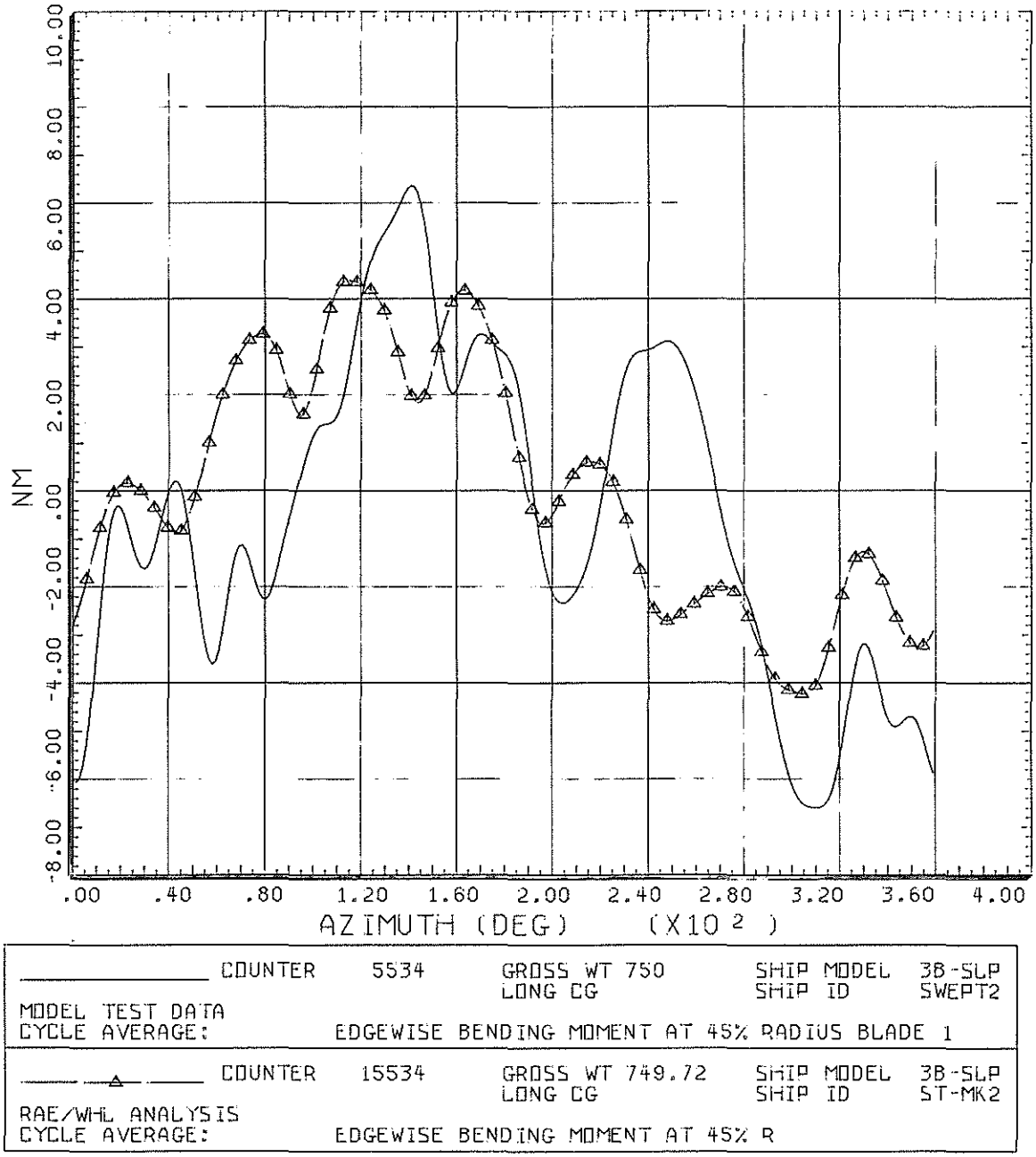

Fig 30 Measured and predicted edgewise bending moment for the model rotor with swept tip blades

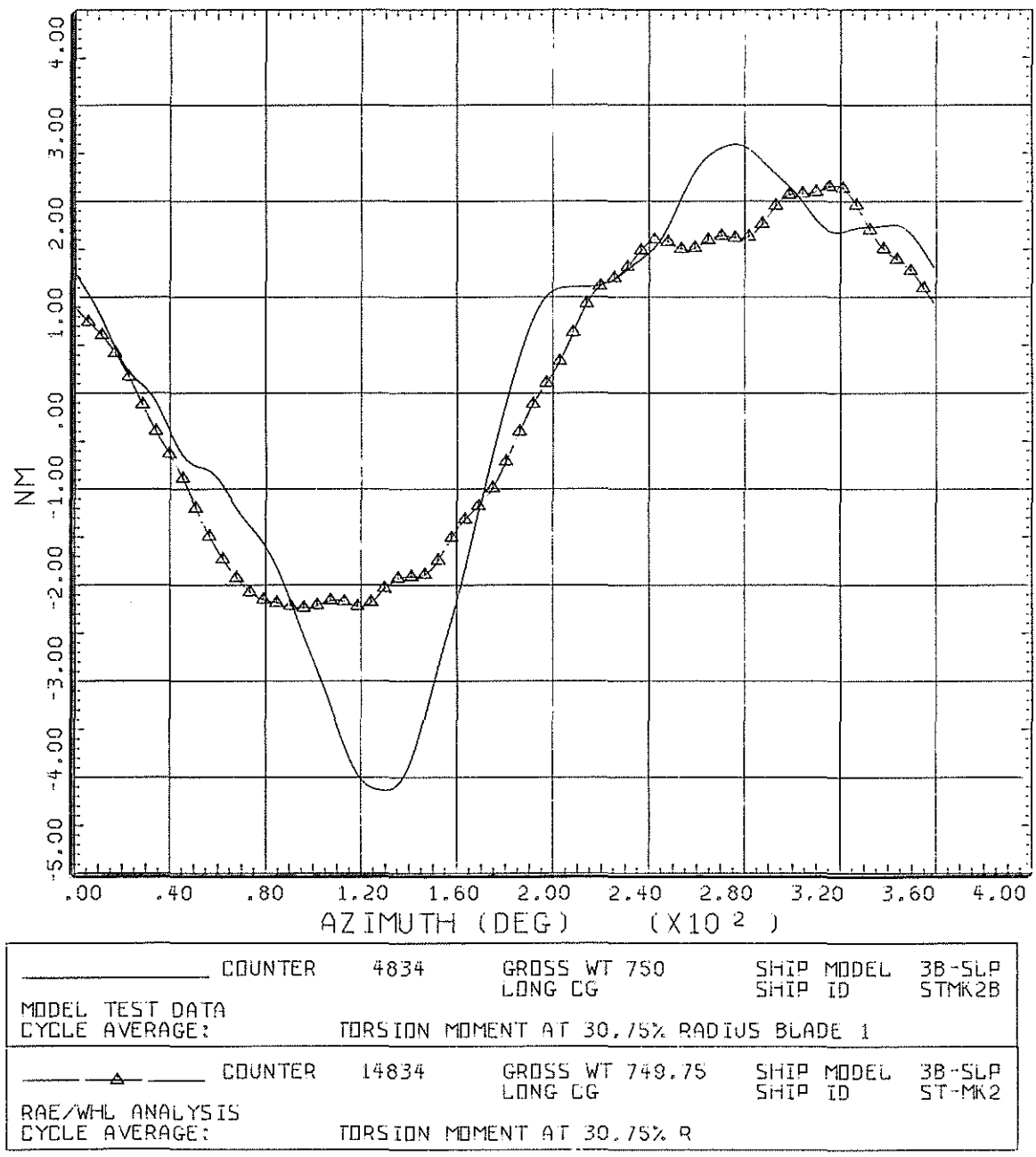

Fig 31 Measured and predicted torsion moment for the model rotor with straight blades

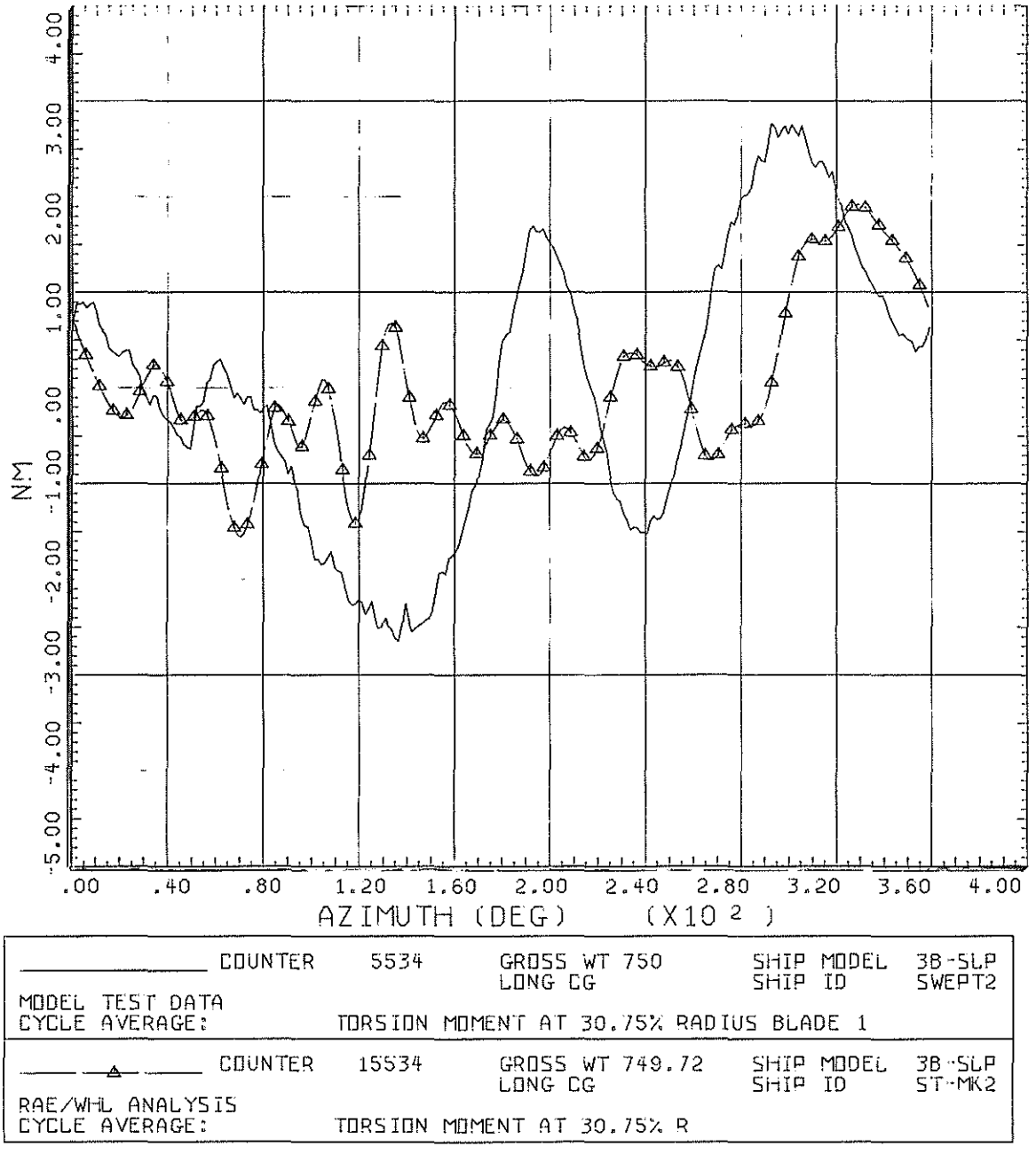

Fig 32 Measured and predicted torsion moment for the model rotor with swept tip blades